

University of Wisconsin - Madison

MADPH-98-1054
HAWAII-511-900-98
VAND-TH-98-05
AMES-HET-98-08
June 1998

VARIATIONS ON FOUR-NEUTRINO OSCILLATIONS

V. Barger¹, S. Pakvasa², T.J. Weiler³, and K. Whisnant⁴

¹*Department of Physics, University of Wisconsin, Madison, WI 53706, USA*

²*Department of Physics and Astronomy, University of Hawaii, Manoa, HI 96822, USA*

³*Department of Physics and Astronomy, Vanderbilt University, Nashville, TN 37235, USA*

⁴*Department of Physics and Astronomy, Iowa State University, Ames, IA 50011, USA*

Abstract

We make a model-independent analysis of all available data that indicate neutrino oscillations. Using probability diagrams, we confirm that a mass spectrum with two nearly degenerate pairs of neutrinos separated by a mass gap of $\simeq 1$ eV is preferred over a spectrum with one mass eigenstate separated from the others. We derive some new relations among the four-neutrino mixing matrix elements. We design four-neutrino mass matrices with three active neutrinos and one sterile neutrino that naturally incorporate maximal oscillations of atmospheric ν_μ and explain the solar neutrino and LSND results. The models allow either a large or small angle MSW or vacuum oscillation description of the solar neutrino deficit. The models predict (i) oscillations of either $\nu_e \rightarrow \nu_\tau$ or $\nu_e \rightarrow \nu_s$ in long-baseline experiments at $L/E \gg 1$ km/GeV, with amplitude determined by the LSND oscillation amplitude and argument given by the atmospheric δm^2 , and (ii) the equality of the ν_e disappearance probability, the ν_μ disappearance probability, and the LSND $\nu_\mu \rightarrow \nu_e$ appearance probability in short-baseline experiments.

1 Introduction

The long-standing solar neutrino deficit [1, 2], the atmospheric neutrino anomaly [3, 4, 5, 6], and the results from the LSND experiment on $\bar{\nu}_e$ neutrinos from μ^+ decay and ν_e neutrinos from π^+ decay [7] can each be understood in terms of oscillations between two neutrino species [8]. Interestingly, the solar, atmospheric, and terrestrial (LSND) neutrino oscillations have different L/E and therefore require different neutrino mass-squared differences δm^2 to properly describe all features of the data. For example, if the atmospheric and LSND δm^2 scales are the same [9], one forfeits the recently reported zenith-angle dependence and up/down asymmetry of the atmospheric neutrino flux [4, 5]. Alternatively, if the solar and atmospheric δm^2 scales [10] are the same, the reduction in the solar neutrino flux is energy-independent, contrary to the three solar experiments which infer different oscillation probabilities in different neutrino energy regions [11]. Since three distinct mass-squared differences cannot be constructed from just three neutrino masses, the collective data thus argue provocatively for more than three oscillating flavors. An alternative but less compelling possibility is to introduce new lepton-flavor changing operators with coefficients small enough to evade present exclusion limits, but large enough to explain the small LSND amplitude [12].

If all of the existing observations are confirmed, a viable solution is to invoke one or more additional species of sterile light neutrino [13], thereby introducing another independent mass scale to the theory. The additional neutrino must be sterile, i.e. without Standard Model gauge interactions, to be consistent with LEP measurements of $Z \rightarrow \nu\bar{\nu}$ [14]. The introduction of a sterile neutrino to complement the three active neutrinos has had some phenomenological success [15].

In this paper we propose and study mass matrices for four-neutrino models (three active plus one sterile) that can accommodate all the present data. Once a fourth neutrino is admitted to the spectrum, it is no longer mandatory that the ν_μ mix with the ν_τ at the atmospheric scale. The ν_μ may instead mix with the sterile ν_s , or with some linear combination of ν_s and ν_τ . Similarly, the ν_e may mix with a linear combination of ν_s and ν_τ .

At first sight the mixing of a sterile neutrino with active flavor neutrinos seems to be stringently constrained by Big Bang nucleosynthesis (BBN) physics. The bound

$$\delta m^2 \sin^2 2\theta < 10^{-7} \text{ eV}^2 \tag{1}$$

on the mass-squared difference δm^2 and the mixing angle of the sterile neutrino was inferred to avoid thermal overpopulation of the “extra” sterile neutrino species [16]. However, there are significant caveats to this bound. One is the fact that some recent estimates of N_ν using higher abundances of ^4He yield considerably weaker bounds [17]. Another is that a small asymmetry $(n_\nu - n_{\bar{\nu}})/n_\gamma \gtrsim 7 \times 10^{-5}$ of flavor neutrinos (but large compared to the present baryon asymmetry $\Delta n_B/n_\gamma \sim 10^{-10}$) at $t > 0.1$ s is enough to suppress $\nu_\mu - \nu_s$ oscillations and then the bound of Eq. (1) does not apply [18]. Such asymmetries, in fact, can be generated with the kind of model parameters considered herein (as shown in Ref. [19, 20]). In light of this observation that BBN may allow sizeable mixing between sterile and active neutrinos, we consider both the small and large mixing with sterile neutrinos in this work.

We review all existing data that indicate neutrino oscillations, and then perform a model-independent analysis of the data using four-neutrino unitarity constraints. A very useful

tool for this unitarity analysis is the set of probability rectangles, which we explain and exploit. We draw several model-independent conclusions for the four-neutrino universe.

We design a five-parameter neutrino mass matrix which can account for each of the three viable solar solutions and accommodate the atmospheric and LSND observations. The three solar possibilities are the small-angle matter-enhanced (SAM) [21, 22, 23, 24], large-angle matter enhanced (LAM) [25] and large-angle vacuum long-wavelength (VLW) [26, 27] explanations of the solar neutrino deficit. Our mass matrix yields maximal oscillations of atmospheric ν_μ . We consider the possibility that the solar data is explained by $\nu_e \rightarrow \nu_s$ or $\nu_e \rightarrow \nu_\tau$ oscillations, in which case the atmospheric neutrino data is explained by either $\nu_\mu \rightarrow \nu_\tau$ or $\nu_\mu \rightarrow \nu_s$ oscillations, respectively. We also consider the possibility that both atmospheric and solar neutrino oscillations have ν_s and ν_τ components. Lack of ν_s - ν_τ discrimination in the present data is the major source of ambiguity in the four-neutrino model. We discuss how future experiments can resolve this ambiguity.

In Sec. 2 we summarize the oscillation probability formulas and utilize a probability formalism, based on unitarity of the mixing matrix, which permits a simple visual representation of mixing. In Sec. 3 we begin with a brief discussion of the three classes of experiments and the neutrino mass and mixing parameters needed to explain them. We then use probability rectangles to display the inferences from the data for any four-neutrino scheme. In Sec. 4 we employ the probability rectangles to argue against a neutrino mass spectrum with one eigenstate separated from three other nearly-degenerate states (which we will refer to as the 1+3 spectrum) in favor of two nearly degenerate mass pairs (which we will refer to as the 2+2 spectrum). We also derive some new relations among elements of the mixing matrix that result from data and unitarity which are satisfied in a four-neutrino model for certain ranges of the parameters. Then in Sec. 5 we present a mass matrix whose eigenvalues consist of a nearly degenerate neutrino pair at ~ 1.4 eV and another nearly degenerate pair at low mass, as illustrated in Fig. 1. We show how the existing data almost uniquely fixes the model parameters (once a solar scenario is specified) and strictly determines what new phenomenology the model predicts. In Sec. 6 we derive expressions for the oscillation probabilities in our models in terms of the current neutrino experimental observables. We present the model predictions in Sec. 7. The new observable signature for the model is $\nu_e \leftrightarrow \nu_\tau$ or $\nu_e \leftrightarrow \nu_s$ oscillations for $L/E \gg 1$ km/GeV, depending on whether the atmospheric oscillations are $\nu_\mu \rightarrow \nu_\tau$ or $\nu_\mu \rightarrow \nu_s$, respectively. Section 8 contains some discussion, and a summary.

2 Formalism

2.1 Oscillation amplitudes

To simplify the analysis of the available data, we will ignore possible CP violation and work with a real-valued mixing matrix U . Accordingly, the general formula for the vacuum oscillation probabilities becomes [28]

$$P(\nu_\alpha \rightarrow \nu_\beta) = \delta_{\alpha\beta} - 4 \sum_{k < j} U_{\alpha k} U_{\beta k} U_{\alpha j} U_{\beta j} \sin^2 \Delta_{jk}, \quad (2)$$

where $\Delta_{jk} \equiv \delta m_{jk}^2 L/4E = 1.27(\delta m_{jk}^2/\text{eV}^2)(L/\text{km})/(E/\text{GeV})$, $\delta m_{jk}^2 \equiv m_j^2 - m_k^2$, and the sum is over all j and k subject to $k < j$.

For oscillations of two neutrinos, the oscillation amplitude (i.e., the coefficient of the $\sin^2 \Delta_{jk}$ term) is given by $\sin^2 2\theta$, where θ is the mixing angle between the two neutrino states. More generally for an arbitrary number of neutrinos, the amplitude of the ν_α to ν_β oscillation in the absence of CP violation is seen to be

$$A^{\alpha\beta} = -4 \sum_{k < j} U_{\alpha j} U_{\beta j} U_{\alpha k} U_{\beta k}, \quad \alpha \neq \beta, \quad (3)$$

where the sum is over mass states with mass-squared differences appropriate for the L/E of the particular experiment. We note that the oscillation amplitudes defined here are only for those oscillations at a particular Δ scale in Eq. (2). We will use subscript labels on the amplitude to identify the Δ scale (which is determined by the relevant δm^2 and L/E) for the particular experiment: “sbl” will denote short-baseline experiments such as LSND, “atm” will denote atmospheric and long-baseline experiments, and “sun” will denote extraterrestrial experiments, especially those with solar neutrinos.

We will use superscripts on the amplitude to identify the oscillation flavors, unless it is obvious from the context; in the absence of CP violation, $A^{\alpha\beta} = A^{\beta\alpha}$. With four neutrino states, U is a 4×4 mixing matrix. We also define the amplitude for ν_α disappearance

$$A^{\alpha\cancel{\alpha}} \equiv \sum_{\beta \neq \alpha} A^{\alpha\beta}, \quad (4)$$

where $\cancel{\alpha}$ represents a sum over neutrino flavor eigenstates other than ν_α . The mixing-matrix elements U , and therefore the amplitudes A , depend on the environment, e.g., matter vs. vacuum. Throughout this paper we will quote values for the oscillation amplitudes *in vacuum*.

2.2 Probability rectangles and a theorem

The “probability rectangles” used by Liu and Smirnov [20] visually illustrate the mixing of the flavor eigenstates among the mass eigenstates. To construct the probability rectangles, we introduce the notation

$$P_{\alpha j} \equiv |U_{\alpha j}|^2, \quad (5)$$

such that $P_{\alpha j}$ is the probability that the α^{th} flavor state is found in the j^{th} mass state, or, alternatively, the probability that the j^{th} mass state is contained in the α^{th} flavor state. Therefore, when CP-violation is neglected, the real mixing-matrix elements are determined by the probabilities up to a sign: $U_{\alpha j} = \pm \sqrt{P_{\alpha j}}$. In principle, these signs may be determined by arranging for orthogonality of the rows, and columns, in the unitary mixing matrix U .

By unitarity of U we have

$$\sum_{\alpha} P_{\alpha j} = 1 \quad (6)$$

for each mass state j , and

$$\sum_j P_{\alpha j} = 1 \quad (7)$$

for each flavor state α . Thus, if each mass state is represented as a rectangle of unit area, then the fractional area assigned to $P_{\alpha j}$ within the rectangle is a graphical representation of

the value of $P_{\alpha j}$. The probabilities $P_{\alpha j}$ depend on whether the environment is vacuum or matter. For consistency, we will always display vacuum probabilities in the rectangles. When the probability rectangles are displayed along a vertical axis labeled with mass-squared, the δm^2 values relevant for the various experiments are readily visualized. Figure 2 gives an example of the probability rectangles for a four-neutrino model. An inverted 2+2 mass spectrum, where the solar ν_e oscillation is driven by the separation of the heavier two states and the atmospheric ν_μ oscillation is driven by the separation of the lighter two states, may also be possible, but is not considered.

The following mini-theorem will prove to be useful:

In the absence of matter effects, the amplitude $A^{\alpha\alpha}$ is independent of how the $P_{\alpha j}$ probabilities are partitioned among the mass eigenstates.

The proof of this statement relies on the insertion of $\sum_{\beta \neq \alpha} U_{\beta j} U_{\beta k} = -U_{\alpha j} U_{\alpha k}$ into $A^{\alpha\alpha} = -4 \sum_{\beta \neq \alpha} \sum_{j,k>j} U_{\alpha j} U_{\alpha k} U_{\beta j} U_{\beta k}$, to get

$$A^{\alpha\alpha} = 4 \sum_{j>k} P_{\alpha j} P_{\alpha k}, \quad (8)$$

where, as in Eq. (3), the sum in Eq. (8) is over all mass states with mass-squared differences appropriate for the L/E of the particular experiment. In Eq. (8), $A_{\alpha\alpha}$ is manifestly independent of the partitioning of the $P_{\alpha j}$ probabilities since it involves only the $P_{\alpha j}$. This theorem demonstrates the limitations on information derivable from disappearance experiments.

The minitheorem fails in the presence of matter effects because the partitioning of the flavor probabilities including $P_{\alpha j}$ are altered. That is, with matter effects the amplitude $A_{\alpha \rightarrow \alpha}$ does depend on how the $P_{\alpha j}$ are partitioned among the mass states. Matter will also alter the oscillation wavelength, causing further changes in the phenomenology of experiments sensitive to the oscillations rather than their averages. Matter effects have the potential to resolve the $\nu_s - \nu_\tau$ ambiguity, as do some other measurements. We discuss these possibilities in Sec. 7.

3 Experimental constraints

3.1 Short baseline: LSND, reactors, and accelerators

The LSND experiment [7] reports positive appearance results for $\bar{\nu}_\mu \rightarrow \bar{\nu}_e$ oscillations from μ^+ decay at rest (DAR) and for $\nu_\mu \rightarrow \nu_e$ oscillations from π^+ decay in flight (DIF). The DAR data has higher statistics, but the allowed regions for the two processes are in good agreement. There are also restrictions from the null results of the BNL E-776 [29] and KARMEN [30] $\nu_\mu \rightarrow \nu_e$ oscillation search experiments. The combined data suggest $\nu_\mu \rightarrow \nu_e$ vacuum oscillation parameters that lie approximately along the line segment described by

$$0.3 \text{ eV}^2 \leq \delta m_{sbl}^2 = \frac{0.030 \text{ eV}^2}{(A_{sbl}^{\mu e})^{0.7}} \leq 2.0 \text{ eV}^2. \quad (9)$$

However, values for δm_{sbl}^2 as high as 10 eV^2 are also allowed for $A_{sbl}^{\mu e} \simeq .0025$, although values above 3 eV^2 are disfavored by the r-process mechanism of heavy element nucleosynthesis in supernovae [31].

There are also relevant data from the Bugey reactor experiment which searches for $\bar{\nu}_e$ disappearance [32], and from the CDHS[33] and CCFR[34] experiments which set bounds on ν_μ disappearance.

The combined short baseline data set for $A^{e\bar{e}}$, $A^{\mu\bar{\mu}}$, and $A^{\mu e}$ will be used in Sec. 4 to argue against a hierarchical neutrino mass spectrum in favor of two pairs of nearly degenerate masses in the four-neutrino spectrum.

3.2 Atmospheric data

The atmospheric neutrino experiments measure ν_μ and ν_e (and their antineutrinos) created when cosmic rays interact with the Earth’s atmosphere. One expects roughly twice as many muon neutrinos as electron neutrinos from the resulting cascade of pion and other meson decays. Several experiments [3, 4] obtain a ν_μ/ν_e ratio that is about 0.6 of the value expected from detailed theoretical calculations of the flux [35]. The Super-Kamiokande (SuperK) experiment has collected the most data and analysis [4] indicates that their results for contained events can be explained as $\nu_\mu \rightarrow \nu_\tau$ oscillations with [4, 6, 36]

$$3 \times 10^{-4} \text{ eV}^2 \leq \delta m_{atm}^2 \leq 7 \times 10^{-3} \text{ eV}^2, \quad 0.8 \leq A_{atm}^{\mu\bar{\mu}} \leq 1.0. \quad (10)$$

The high end of each range is favored.

Independent of flux normalization considerations, the $\nu_\mu \rightarrow \nu_e$ oscillation channel is strongly disfavored by the zenith angle distributions of the data [4] and by the up/down asymmetry separated into “muon-like” (ν_μ) and “electron-like” (ν_e) events [5], which yield an up-to-down ratio of $0.52_{-0.06}^{+0.07} \pm 0.01$ for μ -like events and $0.84_{-0.12}^{+0.14} \pm 0.02$ for e -like events (the expected values are close to unity). Furthermore, the recent CHOOZ $\bar{\nu}_e$ disappearance experiment excludes $\bar{\nu}_e \rightarrow \bar{\nu}_\mu$ oscillations with large mixing $A_{atm}^{\mu\bar{\mu}} \gtrsim 0.2$ for $\delta m_{atm}^2 \geq 10^{-3} \text{ eV}^2$ [37].

In a four-neutrino context, another possibility for the atmospheric neutrino oscillations is $\nu_\mu \rightarrow \nu_s$. Oscillations of this type in principle could be affected by matter due to the different neutral current interactions of ν_μ and ν_s . However, for the contained events (with lower energy) these effects are small, especially for larger values of δm^2 [20, 38]; hence, the allowed regions for $\nu_\mu \rightarrow \nu_s$ should be similar to those for $\nu_\mu \rightarrow \nu_\tau$. For events at higher energies the matter effects could begin to be appreciable; a definitive test requires more data.

3.3 Solar data

The solar neutrino experiments [2] measure ν_e created in the sun. There are three types of experiments, ν_e capture in Cl in the Homestake mine, $\nu_e - e$ scattering at Kamiokande and Super-Kamiokande, and ν_e capture in Ga at SAGE and GALLEX; each is sensitive to different ranges of the solar neutrino spectrum and measures a suppression from the expectations of the standard solar model (SSM)[1].

For $\nu_e \rightarrow \nu_s$ oscillations in the sun (in which case atmospheric neutrino oscillations are $\nu_\mu \rightarrow \nu_\tau$ in our model) the allowed parameter ranges at 95% C.L. [39] for the small-angle matter-enhanced solution are given in Table 1. The solution is based on the SSM fluxes in Ref. [1]. Approximate parameters for the large-angle matter-enhanced [39] and vacuum

long-wavelength solutions [40] for $\nu_e \rightarrow \nu_s$ oscillations of solar neutrinos are also shown in Table 1. If the solar neutrino deficit is caused instead by $\nu_e \rightarrow \nu_\tau$ oscillations (and the atmospheric oscillations are $\nu_\mu \rightarrow \nu_s$), then the allowed solar parameter ranges for the three solar cases are slightly different [39]; see Table 1. The exact values of the parameters may change as new data from SuperK [41] become available and when fits are made with the new solar flux calculations.

In any of the matter-enhanced scenarios it is also necessary that the eigenmass m_1 associated predominantly with ν_e be lighter than the eigenmass m_0 associated predominantly with the neutrino into which the ν_e is oscillating (i.e., ν_s or ν_τ), so that it is ν_e rather than $\bar{\nu}_e$ that is resonant in the sun. For the vacuum solutions the ordering of m_0 and m_1 does not matter. Alternate scenarios where the ν_e is predominantly associated with the heavier two states and ν_μ is predominantly associated with the lighter two states are also viable.

For $\nu_e \rightarrow \nu_\tau$ oscillations in the two-neutrino approximation the propagation equation for the neutrino states in the charge-current basis is [21, 42, 43]

$$i \frac{d}{dt} \begin{pmatrix} \nu_e \\ \nu_\tau \end{pmatrix} = \frac{1}{4E} \begin{pmatrix} 4\sqrt{2}G_F E N_e & \delta m^2 \sin 2\theta \\ \delta m^2 \sin 2\theta & 2\delta m^2 \cos 2\theta \end{pmatrix} \begin{pmatrix} \nu_e \\ \nu_\tau \end{pmatrix}, \quad (11)$$

where N_e is the electron number density. For $\nu_e \rightarrow \nu_s$ oscillations the propagation equation is instead [44]

$$i \frac{d}{dt} \begin{pmatrix} \nu_e \\ \nu_s \end{pmatrix} = \frac{1}{4E} \begin{pmatrix} 4\sqrt{2}G_F E (N_e - \frac{1}{2}N_n) & \delta m^2 \sin 2\theta \\ \delta m^2 \sin 2\theta & 2\delta m^2 \cos 2\theta \end{pmatrix} \begin{pmatrix} \nu_e \\ \nu_s \end{pmatrix}, \quad (12)$$

where N_n is the neutron number density. For the small-angle matter-enhanced case the non-adiabatic approximate solution for neutrino propagation is appropriate and the oscillation probability for a neutrino of energy E_ν is

$$P(\nu_e \rightarrow \nu_\ell) = \frac{1}{2} A_{sun}^{e\ell} + P_x (1 - A_{sun}^{e\ell}) \quad (13)$$

where in this case ℓ labels either τ or s , and

$$P_x = \exp \left[- \frac{\pi \delta m_{sun}^2 (A_{sun}^{e\ell})^2}{4E_\nu \sqrt{1 - A_{sun}^{e\ell}} (d \log N / dL)_c} \right] \quad (14)$$

is the Landau-Zener transition probability and N is either N_e (for $\nu_e \rightarrow \nu_\tau$ oscillations) or $N_e - \frac{1}{2}N_n$ (for $\nu_e \rightarrow \nu_s$ oscillations). The quantity $(d \log N / dL)_c$ is the appropriate logarithmic density gradient in the sun at $N^{crit} = \delta m_{sun}^2 \sqrt{1 - A_{sun}^{e\ell}} / (2\sqrt{2}G_F E_\nu)$, the critical density where maximal oscillations (resonance) occur. For the large-angle matter-enhanced case, the neutrino propagation is adiabatic and

$$P(\nu_e \rightarrow \nu_\ell) = \frac{1}{2} \left[1 - \sqrt{1 - A_{sun}^{e\ell}} \right] \quad (15)$$

assuming the neutrinos are created where the electron density is well above the critical density. For the vacuum long-wavelength solution the oscillation probability is just given by the usual vacuum expressions.

3.4 Oscillation lengths and amplitudes summarized

In neutrino oscillation descriptions of the solar, atmospheric, and LSND data, a distinct oscillation wavelength and oscillation amplitude is required for each of the three data sets. Experimental uncertainties allow for some latitude in these amplitudes and wavelengths, and for the solar data, there are three isolated islands of viability in the δm^2 -amplitude plane [45]; see Fig. 3. The day–night asymmetry measurement, found to be small in the recent SuperK data, removed about half of the previously viable solar regions [45].

The vacuum oscillation wavelength is linear in the neutrino energy, allowing further possibilities that are summarized in Table 2. The chosen neutrino energies are typical for solar, and reactor sources (5 MeV), pion facilities (100 MeV), for contained (2 GeV), partially–contained (10 GeV), and throughgoing (100 GeV) neutrino events in underground detectors, and for astrophysical sources (1 TeV). Although full oscillation wavelengths are also listed in Table 2, oscillation effects may well be measurable for a fraction of an oscillation wavelength or as an average over many oscillation wavelengths. Throughgoing and partially contained atmospheric neutrinos may show nodes as a function of L/E . Further possibilities arise when the matter effect of the earth is included in the oscillation physics. We consider earth–matter effects in Sec. 7.6.

3.5 Inferences from data

We consider first the probability rectangles for the atmospheric and CHOOZ data. The atmospheric data indicate $\delta m_{atm}^2 \sim 5 \times 10^{-3}$ and nearly maximal flavor–changing mixing of ν_μ with ν_ϕ . The present data do not distinguish between ν_τ or ν_s as the dominant state into which ν_μ mixes. The probability rectangles for the atmospheric scale are displayed in Fig. 4a. We label the two masses defining the atmospheric scale as ν_2 and ν_3 , with $\delta m_{atm}^2 = \delta m_{32}^2$. Because of the “ ν_τ – ν_s ” ambiguity we show the union $P_\tau + P_s$ rather than the partitions into P_τ and P_s . For maximal ν_μ – ν_ϕ mixing, one must choose $P_{\mu 2} \sim P_{\mu 3} \sim P_{\tau 2} + P_{s 2} \sim P_{\tau 3} + P_{s 3} \sim 1/2$.

Next we consider the pair of mass eigenstates whose mass–squared difference is fixed by the solar scale. We provisionally investigate a four–neutrino mass spectrum that consists of two pairs of nearly degenerate neutrinos separated by the LSND scale $\delta m_{sbl}^2 \sim \text{eV}^2$ (to explain the LSND result in terms of oscillations). We argue in Sec. 4 that the data favor this spectrum over a spectrum with one mass separated from three relatively degenerate masses. We label the second pair of mass states as ν_0 and ν_1 , and define $\delta m_{sun}^2 = \delta m_{10}^2$. Since $P_{\mu 2}$ and $P_{\mu 3}$ sum to near unity, $P_{\mu 0}$ and $P_{\mu 1}$ must be small. Thus the probability rectangles for the ν_0 and ν_1 states appear as shown in Fig. 4a. Accordingly, the LSND amplitude for $\nu_\mu \rightarrow \nu_e$,

$$A_{sbl}^{\mu e} = -4 [U_{\mu 3} U_{e 3} + U_{\mu 2} U_{e 2}] [U_{\mu 1} U_{e 1} + U_{\mu 0} U_{e 0}], \quad (16)$$

is necessarily small. We emphasize that the smallness of the LSND ν_e – ν_μ mixing is an inevitable consequence of the large mixing of ν_μ to ν_ϕ at the atmospheric scale and the constraints of unitarity, independent of particular model considerations including rearrangement of the neutrino mass spectrum.

Four–neutrino unitarity may be used to rewrite eqn. (16) as

$$A_{sbl}^{\mu e} = 4 |U_{\mu 3} U_{e 3} + U_{\mu 2} U_{e 2}|^2 = 4 |U_{\mu 1} U_{e 1} + U_{\mu 0} U_{e 0}|^2. \quad (17)$$

Written this way, it is clear that the LSND data is blind to the partitioning of ν_τ and ν_s in the probability rectangles of mass states ν_0 and ν_1 . This flavor ambiguity is shown in Fig. 4a.

With the identification $\delta m_{sun}^2 = \delta m_{10}^2$, we may use Eq. (8) to write the solar ν_e -disappearance amplitude as

$$A_{sun}^{e\ell} = 4 P_{e0} P_{e1}. \quad (18)$$

Because matter in the sun may exert a significant effect on propagating neutrinos, the values of P_{e0} and P_{e1} for the sun have some sensitivity to the state ν_τ or ν_s into which ν_e oscillates. However, the sensitivity of present data to this difference is weak, and there is considerable freedom in assigning ν_τ or ν_s or a linear combination thereof as the mixing partner to ν_e . This ν_τ - ν_s ambiguity for ν_e mixing at the solar scale is complementary to the ν_s - ν_τ ambiguity for ν_μ mixing at the atmospheric scale. Potential measurements to resolve the ν_s - ν_τ ambiguity at the solar scale will be discussed in Sec. 7.

3.6 The three solar solutions

The P_{e0} and P_{e1} partitioning specifies whether the solar model is a small-angle model or a large-angle model. As can be inferred from Eq. (18), with nearly-equal partitioning of P_{e0} and P_{e1} , the mixing amplitude is near maximal (large angle). With highly nonequal partitioning, i.e., $P_{e0} \ll P_{e1}$ or $P_{e1} \ll P_{e0}$, the mixing amplitude is small. Of the three viable solar neutrino options, SAM falls into the small angle category, while LAM and VLW fall into the large angle category. The probability rectangles for the small and large angle classes of models are shown in Figs. 4b and 4c. Recall that in order to obtain the MSW resonant enhancement required for the SAM and LAM solutions, it is necessary that the state which is predominantly ν_e be the lighter of the two mass states, ν_1 . Qualitatively, LAM and VLW are distinguishable in their probability rectangles only by the choice of value for δm_{sun}^2 . Quantitatively, the two solutions and the VLW solution are distinguishable in ways which are discussed in Sec. 7.

If the active-sterile mixing is small, then all ambiguities in the probability rectangles are resolved: the large atmospheric mixing must be ν_μ - ν_τ , and the solar solution must be small-angle SAM with ν_e - ν_s mixing. The probability rectangles for this model are shown in Fig. 2. This particular solution has recently been analyzed in the context of the minimal four-neutrino mass matrix [46, 47].

4 Mass spectra

4.1 Argument against a 1+3 mass spectrum

It has been shown by Bilenky, Giunti and Grimus [48] that a hierarchical ordering of the four-neutrino spectrum (implying one dominant mass) is disfavored by the data when the null results of reactor and accelerator disappearance experiments are included. We will refer to this spectrum as the 1+3 spectrum, defined as one heavier mass state separated from three lighter, nearly-degenerate states, or vice versa. We demonstrate the argument with a set of logical steps similar to theirs.

Assume a mass spectrum with one heavy mass well separated from three other nearly-degenerate states and let the heavy mass state be labeled as ν_3 . Then the LSND mass-squared scale is $\delta m_{sbl}^2 \simeq \delta m_{32}^2 \simeq \delta m_{31}^2 \simeq \delta m_{30}^2$ and the LSND amplitude is

$$A_{sbl}^{\mu e} = -4 U_{e3} U_{\mu 3} \left[\sum_{j \neq 3} U_{\mu j} U_{ej} \right] = 4 P_{e3} P_{\mu 3}, \quad \text{with } P_{e3} + P_{\mu 3} \leq 1. \quad (19)$$

On the other hand, the ν_e and ν_μ disappearance experiments at reactors and accelerators are also sensitive to the LSND scale. These experiments measure the disappearance amplitudes

$$A_{sbl}^{e\ell} = 4 P_{e3} \left[\sum_{j \neq 3} P_{ej} \right] = 4 P_{e3} [1 - P_{e3}] \quad (20)$$

and

$$A_{sbl}^{\mu\ell} = 4 P_{\mu 3} [1 - P_{\mu 3}]. \quad (21)$$

The second equalities in Eqs. (19) and (20) (see Eq. (8)) follow from unitarity of the mixing matrix. The three amplitudes in Eqs. (19)–(21) depend on just two parameters, and so are interrelated. All three of these amplitudes are constrained by experiments to be small. *A priori* then, P_{e3} and $P_{\mu 3}$ may both be small, or one (but not both) may be near unity with the other small. The fact that $A_{sbl}^{\mu e}$ is an *appearance observation* rather than a bound means that if P_{e3} and $P_{\mu 3}$ are both small, they cannot be too small.

In the 1+3 model, the atmospheric scale does not involve the heavy state ν_3 . Without loss of generality we label the state which determines the atmospheric scale as ν_2 . Then from Eq. (8) the atmospheric ν_μ disappearance oscillation amplitude is given by

$$A_{atm}^{\mu\ell} = 4 P_{\mu 2} (P_{\mu 0} + P_{\mu 1}) \leq (1 - P_{\mu 3})^2, \quad (22)$$

where the inequality comes from maximizing $4 P_{\mu 2} (P_{\mu 0} + P_{\mu 1})$ subject to the constraint $P_{\mu 0} + P_{\mu 1} + P_{\mu 2} = 1 - P_{\mu 3}$. The SuperK data indicate that ν_μ is maximally mixed at the δm_{atm}^2 scale, i.e., there is little ν_μ -content available to the ν_3 state. Quantitatively we have $A_{atm}^{\mu\ell} \geq 0.8$, which implies $P_{\mu 3} \leq 0.11$. Since $P_{\mu 3}$ is small, Eq. (21) becomes

$$A_{sbl}^{\mu\ell} \simeq 4 P_{\mu 3} \ll 1. \quad (23)$$

The probability rectangles for the 1+3 model with small $P_{\mu 3}$ are presented in Fig. 5. Note that it is the zenith-angle, or up/down asymmetry data, which really establishes δm_{atm}^2 as different from δm_{sbl}^2 , that is crucial for the argument [48].

We are left with the possibilities of P_{e3} being small or near unity. As can be seen in Fig. 5, if P_{e3} is near unity, then there is little $P_{e\beta}$ to distribute over the three lighter mass states. In particular, the solar amplitude $A_{sun}^{e\ell} = 4 P_{e0} P_{e1}$, where the solar scale is $\delta m_{sun}^2 = \delta m_{10}^2$, is second order in small quantities, too small for even the SAM solution ($A_{SAM} \geq 2.5 \times 10^{-3}$) to the solar flux. This may be easily quantified. If P_{e3} were near unity, we would have

$$A_{sbl}^{e\ell} \simeq 4 [1 - P_{e3}] \ll 1. \quad (24)$$

Together with unitarity, this in turn bounds the magnitude of the solar amplitude:

$$A_{sun}^{e\ell} = 4 P_{e0} P_{e1} \leq (1 - P_{e3})^2 \simeq \frac{1}{16} (A_{sbl}^{e\ell})^2, \quad (25)$$

where the inequality in Eq. (25) comes from maximizing $4P_{e0}P_{e1}$ subject to the constraint $P_{e0} + P_{e1} \leq 1 - P_{e3}$. The experimental upper limit on $A_{sbl}^{e\ell}$ from the BUGEY experiment [32] is about 0.1 for $\delta m_{sbl}^2 \leq 2 \text{ eV}^2$, which disallows even the small-angle solar solution. We conclude that P_{e3} is small, in which case

$$A_{sbl}^{e\ell} \simeq 4 P_{e3} \ll 1. \quad (26)$$

Thus, both P_{e3} and $P_{\mu 3}$ must be small in the 1+3 model, and from Eqs. (19), (23), and (26), we infer the relation

$$A_{sbl}^{\mu e} \simeq \frac{1}{4} A_{sbl}^{\mu\mu} A_{sbl}^{e\ell}. \quad (27)$$

However, the experimental upper bounds on the disappearance amplitudes $A_{sbl}^{e\ell}$ [32] and $A_{sbl}^{\mu\mu}$ [33] and the measured appearance result for $A_{sbl}^{\mu e}$ [7] are not compatible with Eq. (27), thereby disfavoring the 1+3 model. For example, for $\delta m_{sbl}^2 = 0.3 \text{ eV}^2$, $A_{sbl}^{e\ell} < 0.035$ from Bugey, $A_{sbl}^{\mu\mu} < 0.8$ from CDHS, which implies $A_{sbl}^{\mu e} < 0.007$; however, for this value of δm_{sbl}^2 , the LSND data indicate $A_{sbl}^{\mu e} > 0.04$. The LSND results are presented in terms of maximum likelihood rather than confidence level limits, so it is not straightforward to state an exclusion probability.

Put another way, $A_{sbl}^{\mu e}$ is large enough that the Bugey and CDHS limits force one of P_{e3} and $P_{\mu 3}$ to be small and the other to be large, but this is ruled out by the solar and atmospheric data. The constraints on P_{e3} and $P_{\mu 3}$ from the three short-baseline amplitudes $A_{sbl}^{e\mu}$, $A_{sbl}^{e\ell}$, and $A_{sbl}^{\mu\mu}$, the atmospheric amplitude $A_{atm}^{\mu\mu}$ and the solar amplitude $A_{sun}^{e\ell}$ (from Eqs. (19), (20), (21), (22), and (25), respectively) are conveniently summarized in Fig. 6 for two different values of δm_{sbl}^2 .

The measured values and bounds for the short-baseline appearance and disappearance amplitudes depend on the magnitude of δm_{sbl}^2 . (There is effectively a suppressed δm_{sbl}^2 third axis in our Fig. 6, which samples only two particular values of δm_{sbl}^2 .) For certain allowed values of δm^2 (e.g., at 1.7 eV^2 and 0.25 eV^2 according to Fig. 2 of [48]) the violation of Eq. (27) is mild, and the 1+3 model is just barely incompatible with the data; see, e.g., Fig. 6a.

The argument against the 1+3 model does not depend on the sign of δm_{sbl}^2 . This means that the inverted 3+1 model with the three nearly degenerate mass states heavier than the remaining state is equally disfavored.

4.2 2+2 mass spectrum

We now turn to the favored class of four-neutrino models, namely those with two nearly degenerate mass pairs separated by the LSND scale as displayed in Fig. 1. It is interesting to see how this ‘‘pair of pairs’’ mass spectrum of four-neutrino models realizes the dependency among $A_{sbl}^{\mu e}$, $A_{sbl}^{\mu\mu}$, and $A_{sbl}^{e\ell}$ which conflicted with the 1+3 model. Let ν_0 and ν_1 label the pair of the nearly-degenerate mass eigenstates responsible for the solar oscillations, and ν_2 and ν_3 label the pair of the nearly-degenerate mass eigenstates responsible for the atmospheric oscillations.

The expressions for the oscillation amplitudes are

$$A_{sbl}^{\mu e} = 4 |U_{e2}U_{\mu 2} + U_{e3}U_{\mu 3}|^2 = 4 |U_{e0}U_{\mu 0} + U_{e1}U_{\mu 1}|^2, \quad (28)$$

$$A_{sbl}^{e\ell} = 4(P_{e3}P_{e1} + P_{e3}P_{e0} + P_{e2}P_{e1} + P_{e2}P_{e0}) = 4\sigma_e(1 - \sigma_e), \quad (29)$$

and

$$A_{sbl}^{\mu\ell} = 4(P_{\mu3}P_{\mu1} + P_{\mu3}P_{\mu0} + P_{\mu2}P_{\mu1} + P_{\mu2}P_{\mu0}) = 4\sigma_\mu(1 - \sigma_\mu), \quad (30)$$

with

$$\sigma_\alpha \equiv |U_{\alpha2}|^2 + |U_{\alpha3}|^2 = P_{\alpha2} + P_{\alpha3}. \quad (31)$$

The Schwartz vector inequality $|\vec{v}_e \cdot \vec{v}_\mu|^2 \leq |\vec{v}_e|^2 |\vec{v}_\mu|^2$ applied to the vectors $\vec{v}_e \equiv (U_{e2}, U_{e3})$ and $\vec{v}_\mu \equiv (U_{\mu2}, U_{\mu3})$ then gives

$$A_{sbl}^{\mu e} \leq 4\sigma_e\sigma_\mu. \quad (32)$$

Furthermore, in the 2+2 model the solar oscillation amplitude is

$$A_{sun}^{e\ell} = 4P_{e0}P_{e1} \leq (1 - \sigma_e)^2, \quad (33)$$

and the atmospheric oscillation amplitude is

$$A_{atm}^{\mu\ell} = 4P_{\mu2}P_{\mu3} \leq \sigma_\mu^2, \quad (34)$$

where the inequalities in Eqs. (33) and (34) come from maximizing the expressions subject to the constraints $P_{e0} + P_{e1} = 1 - \sigma_e$ and $P_{\mu2} + P_{\mu3} = \sigma_\mu$, respectively.

If the vector inequality in Eq. (32) is saturated, then $A_{sbl}^{e\mu}$, $A_{sbl}^{e\ell}$, and $A_{sbl}^{\mu\ell}$ each has the same functional dependence on two parameters as it did in the 1+3 model (σ_e has replaced P_{e3} and σ_μ has replaced $P_{\mu3}$). Then the previous argument that the LSND, Bugey and CDHS data require one parameter to be small ($\ll 1$) and the other large ($\simeq 1$) applies. The argument is unaffected if the vector inequality is not saturated. As before in the 1+3 case, the solar constraint indicates that σ_e must be small. This time however, unlike the 1+3 case, the atmospheric constraint involves σ_μ^2 and not $(1 - \sigma_\mu)^2$, and can be met if σ_μ is large ($\simeq 1$). Therefore the constraints of the data can be satisfied by assigning ν_e dominantly to one pair of mass states and ν_μ dominantly to the other pair. Instead of Eq. (27) pertinent to the 1+3 spectrum, we obtain for the 2+2 spectrum

$$A_{sbl}^{\mu e} \leq A_{sbl}^{e\ell}. \quad (35)$$

This bound is linear in the small disappearance amplitudes, and is easily satisfied by the data. For example, the tightest constraint on $A_{sbl}^{e\ell}$ is about 0.02 for $\delta m_{sbl}^2 = 0.6 \text{ eV}^2$, while the LSND data indicate $A_{sbl}^{\mu e}$ can be as low as 0.009 for this value of δm_{sbl}^2 .

In Fig. 7 we have drawn the σ_e - σ_μ plot for the 2+2 model, analogous to the P_{e3} - $P_{\mu3}$ plot for the 1+3 model, for $\delta m_{sbl}^2 = 1.7 \text{ eV}^2$. The allowed regions with σ_μ near unity (implying near-maximal mixing of ν_μ in the ν_2 - ν_3 pair) and σ_e small (implying almost no mixing of ν_e into the ν_2 - ν_3 pair) show that the 2+2 model can comfortably accommodate the data.

Since only mass-squared differences are important for oscillations, the inverted 2+2 model, where the solar oscillations are driven by the mass-squared difference of the upper mass pair and the atmospheric oscillations are driven by the mass-squared difference of the lower mass pair, is equally viable.

4.3 New results

Two features of the data are especially noteworthy. The first is the remarkably high degree of isolation of ν_e into one mass pair and ν_μ into the other mass pair, as inferred from the bounds on the disappearance amplitudes. The second is the near saturation of the vector inequality in Eq. (32) by the LSND appearance amplitude $A_{sbl}^{\mu e}$ for $\delta m_{sbl}^2 \simeq 0.3 \text{ eV}^2$.

Equations (29) and (30) bound the degree to which ν_e and ν_μ are found in opposite pairs of mass eigenstates. Without loss of generality we assume that ν_e is predominantly associated with ν_0 and ν_1 , and that ν_μ is predominantly associated with ν_2 and ν_3 . Then from the Bugey and CDHS data we find the constraints

$$\sigma_e \simeq \frac{1}{4} A_{sbl}^{e\ell} \leq 0.016 (0.009), \quad (36)$$

and

$$1 - \sigma_\mu \simeq \frac{1}{4} A_{sbl}^{\mu\mu} \leq 0.013 (0.2), \quad (37)$$

respectively, for $\delta m_{sbl}^2 = 2 \text{ eV}^2$ (0.3 eV^2). We then deduce

$$A_{sbl}^{e\ell} \leq 0.065 (0.04), \quad (38)$$

which can be compared to the LSND data

$$A_{sbl}^{\mu e} \simeq 0.0025 (0.04), \quad (39)$$

for these two values of δm_{sbl}^2 . The near-saturation of the inequality in Eq. (35) for $\delta m_{sbl}^2 = 0.3 \text{ eV}^2$ has very interesting implications. It means that \hat{v}_e is nearly parallel or antiparallel to \hat{v}_μ , which in turn indicates that

$$|U_{e2}/U_{e3}| \simeq |U_{\mu2}/U_{\mu3}|. \quad (40)$$

This is a new result.

Furthermore, the SuperK data suggest that ν_μ is maximally mixed in the mass pair with mass-squared difference δm_{atm}^2 , so for this pair, called ν_2 and ν_3 , that

$$|U_{\mu2}| \simeq |U_{\mu3}| \simeq \frac{1}{\sqrt{2}}. \quad (41)$$

Then Eq. (40) implies

$$|U_{e2}| \simeq |U_{e3}|. \quad (42)$$

This is also a new result. In summary, if the oscillation parameters are indeed near the limits of the Bugey bound, the four-neutrino mixing matrix in the 2+2 model must satisfy Eq. (40), which implies Eq. (42) if the atmospheric ν_μ mixing is maximal.

We can derive additional constraints by considering $\sigma'_e = P_{e0} + P_{e1}$ and $\sigma'_\mu = P_{\mu0} + P_{\mu1}$ rather than σ_e and σ_μ . The data requires σ'_e to be large ($\simeq 1$) and σ'_μ small, and the Schwartz inequality reduces to

$$A_{sbl}^{\mu e} \leq A_{sbl}^{\mu\mu}, \quad (43)$$

where the CDHS bound is

$$A_{sbl}^{\mu\mu'} \leq 0.05 \text{ (0.8)}, \quad (44)$$

at $\delta m_{sbl}^2 = 2.0 \text{ eV}^2$ (0.3 eV²). Because the inequality in Eq. (43) is not saturated by the data for any δm_{sbl}^2 , a relation similar to Eq. (40) for U_{e0} , U_{e1} , $U_{\mu 0}$, and $U_{\mu 1}$ is not required in the 2+2 model. However, the explicit mass matrices we consider do have such additional relations; see Sec. 5.

Finally, we mention a curiosity [49] in the data which occurs for the pair of pairs mass spectrum with the matter-enhanced solar solutions (SAM and LAM). The *linear* mass splitting at the heavier pair is $m_3 - m_2 \sim \delta m_{32}^2 / 2m_3$. If this pair is associated with the atmospheric scale, we have $m_3 - m_2 \sim 2.5 \times 10^{-2} \text{ eV} (\delta m_{atm}^2 / 5 \times 10^{-3} \text{ eV}^2) (m_3 / \text{eV})^{-1}$. On the other hand, if the lighter mass pair is associated with the matter-enhanced solar scale, and $m_0 \gg m_1$, then the linear mass-splitting of this pair is $m_0 - m_1 \sim m_0 \sim \sqrt{\delta m_{sun}^2} = 2.5 \times 10^{-2} \text{ eV} (\delta m_{sun}^2 / 10^{-5} \text{ eV}^2)^{\frac{1}{2}}$. The two linear mass splittings within the pairs are nearly identical. While squared masses enter into the oscillation formulae for relativistic neutrinos, the more fundamental constructs of field theory, such as the Lagrangian and the resulting equations of motion, are linear in fermion masses (and quadratic in boson masses, these powers of mass being related to the dimensionality of the fermion field vs. the boson field). Thus it is a worthy enterprise to attempt to deduce linear neutrino-mass relations whenever possible.

5 Mass matrix ansatzes

5.1 Solar $\nu_e \rightarrow \nu_s$ oscillations

To describe the above oscillation phenomena in the scenario where the solar neutrino deficit is described by $\nu_e \rightarrow \nu_s$ oscillations and the atmospheric data by $\nu_\mu \rightarrow \nu_\tau$, we consider the neutrino mass matrix ansatz

$$M = m \begin{pmatrix} \epsilon_1 & \epsilon_2 & 0 & 0 \\ \epsilon_2 & 0 & 0 & \epsilon_3 \\ 0 & 0 & \epsilon_4 & 1 \\ 0 & \epsilon_3 & 1 & \epsilon_4 \end{pmatrix}, \quad (45)$$

presented in the $(\nu_s, \nu_e, \nu_\mu, \nu_\tau)$ basis (i.e. the basis where the charged lepton mass matrix is diagonal). By considering the field redefinitions $\Psi \rightarrow -\Psi$ and $\Psi \rightarrow \gamma_5 \Psi$ one realizes that m , and at least one of ϵ_1 and ϵ_4 , and at least one of ϵ_2 and ϵ_3 , may be taken as positive; we will take m and all four ϵ_j to be positive for simplicity. The mass matrix M contains five parameters ($m, \epsilon_1, \epsilon_2, \epsilon_3, \epsilon_4$), just enough to incorporate the required three mass-squared differences and the oscillation amplitudes for solar and LSND neutrinos. The large amplitude for atmospheric oscillations does not require a sixth parameter in our model because the structure of the mass matrix naturally gives maximal mixing of ν_μ with ν_τ (or with ν_s if ν_τ and ν_s are interchanged).

For simplicity, we have taken the mass matrix to be real and symmetric. The choice of a symmetric neutrino mass matrix is well-motivated in the context of oscillations, for what is

measured in neutrino oscillations are the differences of squared masses, which are eigenvalues of the hermitian matrix MM^\dagger , which is itself symmetric when CP conservation is assumed. M is diagonalized by an orthogonal matrix U (real) and there is no CP violation. The ϵ_j are assumed to be small compared to unity, but not all necessarily of the same order of magnitude. The zero terms in the mass matrix could be taken as nonzero without changing the phenomenology discussed here as long as they are small compared to the terms shown. Also, the $M_{\nu_\mu\nu_\mu}$ term could be chosen different from ϵ_4 while still giving maximal mixing of ν_μ and ν_τ since maximal mixing results from the large value of the $M_{\nu_\mu\nu_\tau}$ matrix element relative to the diagonal $M_{\nu_\mu\nu_\mu}$ and $M_{\nu_\tau\nu_\tau}$ elements, without any need for fine tuning of the difference $|M_{\nu_\mu\nu_\mu} - M_{\nu_\tau\nu_\tau}|$. Here we choose to take the minimal form for M needed to describe the data and then derive the associated consequences.

To a good approximation, the two large eigenvalues of the mass matrix in Eq. (45) are

$$m_{2,3} = \mp m \left(1 \mp \epsilon_4 + \frac{1}{2}\epsilon_3^2 \right) . \quad (46)$$

The values of the two small eigenvalues depend on the hierarchy of the ϵ_j . For the three solar cases we have:

$$\text{SAM : } \quad \epsilon_2 \ll \epsilon_1, \epsilon_4 \ll \epsilon_3 \ll 1 , \quad (47)$$

$$\text{LAM : } \quad \epsilon_1, \epsilon_2, \epsilon_4 \ll \epsilon_3 \ll 1 , \quad (48)$$

$$\text{VLW : } \quad \epsilon_1 \ll \epsilon_2 \ll \epsilon_4 \ll \epsilon_3 \ll 1 . \quad (49)$$

The two small eigenvalues are then approximately given by

$$\text{SAM : } \quad m_0 \simeq m\epsilon_1 , \quad m_1 \simeq m(\epsilon_3^2\epsilon_4 - \epsilon_2^2/\epsilon_1) , \quad (50)$$

$$\text{LAM : } \quad m_{0,1} \simeq \frac{m}{2} \left[\epsilon_1 \pm \sqrt{\epsilon_1^2 + 4\epsilon_2^2} \right] , \quad (51)$$

$$\text{VLW : } \quad m_{0,1} \simeq m \left[\pm\epsilon_2 + \epsilon_3^2\epsilon_4/2 \right] . \quad (52)$$

These approximate expressions for the eigenvalues have been obtained by multiplying each ϵ_j by powers of a hypothetical parameter δ , where the number of powers of δ assigned to each ϵ_j depends upon the ordering in Eqs. (47)-(49). For example, in the SAM case ϵ_3 are multiplied by δ , ϵ_1 and ϵ_4 by δ^2 , and ϵ_2 by δ^3 . Then each eigenvalue is written as an expansion in powers of δ , the coefficients of which may be solved for by requiring that the expression $\Pi_i(\lambda - \lambda_i)$ reproduces the eigenvalue equation for the mass matrix order by order in δ . Once the coefficients are found, δ is set equal to unity.

The eigenvalues in all cases have the desired hierarchy $m_1 < m_0 \ll m_2, m_3$, which gives the mass spectrum of the 2+2 model described in Sec. 4.2 and depicted in Fig. 1. The small relative mass splitting of the heavier masses m_2, m_3 is governed entirely by the parameter ϵ_4 : $\delta m_{32}^2 \simeq 4m^2\epsilon_4$. The LSND $\nu_\mu \rightarrow \nu_e$ oscillations are driven by the scale $\delta m_{21}^2 \simeq \delta m_{31}^2 \simeq \delta m_{20}^2 \simeq \delta m_{30}^2 \simeq m^2$, the atmospheric ν_μ oscillations are determined by δm_{32}^2 , and the solar $\nu_e \rightarrow \nu_s$ oscillations are determined by δm_{10}^2 , the approximate expression for which can be obtained by Eqs. (50)-(52). The charged-current eigenstates are approximately

related to the mass eigenstates by

$$\begin{pmatrix} \nu_s \\ \nu_e \\ \nu_\mu \\ \nu_\tau \end{pmatrix} = U \begin{pmatrix} \nu_0 \\ \nu_1 \\ \nu_2 \\ \nu_3 \end{pmatrix} \simeq \begin{pmatrix} \cos \theta & -\sin \theta & \cdots & \cdots \\ \sin \theta & \cos \theta & \frac{1}{\sqrt{2}}\epsilon_3 & \frac{1}{\sqrt{2}}\epsilon_3 \\ -\epsilon_3 \sin \theta & -\epsilon_3 \cos \theta & \frac{1}{\sqrt{2}} & \frac{1}{\sqrt{2}} \\ \cdots & \cdots & -\frac{1}{\sqrt{2}} & \frac{1}{\sqrt{2}} \end{pmatrix} \begin{pmatrix} \nu_0 \\ \nu_1 \\ \nu_2 \\ \nu_3 \end{pmatrix}, \quad (53)$$

where $\tan 2\theta = 2\epsilon_2/\epsilon_1$. The dots indicate nonzero terms that are much smaller than the terms shown. It is their smallness that suppresses mixing between ν_τ and ν_s . The mixing matrix U depends on just three of the original five parameters; it is independent of ϵ_4 and the overall mass-scale parameter m . Note that ν_0 and ν_1 couple predominantly to ν_s and ν_e . The nearly-degenerate ν_2 and ν_3 are seen to consist primarily of nearly equal mixtures of ν_μ and ν_τ . These results, illustrated in Fig. 2, conform to the qualitative arguments of Sec. 3 based on probability rectangles.

It is noted that this mixing matrix not only satisfies the approximate equalities of Eqs. (40)–(42), but in fact replaces the approximate equalities, derived from parameter-independent arguments, with exact equalities to first order in ϵ_j . Inspection of the mixing matrix reveals that our model predicts saturation of Eqs. (35) and (43) to this order, i.e., $A_{sbl}^{e\ell} = A_{sbl}^{\mu\ell} = A_{sbl}^{\nu e}$. A small improvement in the measurement of $A_{sbl}^{e\ell}$ or a modest improvement in the measurement of $A_{sbl}^{\mu\ell}$ is predicted to show a positive disappearance signal.

5.2 Solar $\nu_e \rightarrow \nu_\tau$ oscillations

Another scenario, with solar $\nu_e \rightarrow \nu_\tau$ and atmospheric $\nu_\mu \rightarrow \nu_s$ oscillations, is readily obtained by interchanging $\nu_\tau \rightarrow \nu_s$ and $\nu_s \rightarrow -\nu_\tau$. The mass matrix in the $(\nu_s, \nu_e, \nu_\mu, \nu_\tau)$ basis is then

$$M = m \begin{pmatrix} \epsilon_4 & \epsilon_3 & 1 & 0 \\ \epsilon_3 & 0 & 0 & -\epsilon_2 \\ 1 & 0 & \epsilon_4 & 0 \\ 0 & -\epsilon_2 & 0 & \epsilon_1 \end{pmatrix}. \quad (54)$$

The eigenvalues and parameter hierarchies are still given by Eqs. (46)–(52). The mixing matrix is then given by

$$\begin{pmatrix} \nu_s \\ \nu_e \\ \nu_\mu \\ \nu_\tau \end{pmatrix} = U \begin{pmatrix} \nu_0 \\ \nu_1 \\ \nu_2 \\ \nu_3 \end{pmatrix} \simeq \begin{pmatrix} \cdots & \cdots & -\frac{1}{\sqrt{2}} & \frac{1}{\sqrt{2}} \\ \sin \theta & \cos \theta & \frac{1}{\sqrt{2}}\epsilon_3 & \frac{1}{\sqrt{2}}\epsilon_3 \\ -\epsilon_3 \sin \theta & -\epsilon_3 \cos \theta & \frac{1}{\sqrt{2}} & \frac{1}{\sqrt{2}} \\ -\cos \theta & \sin \theta & \cdots & \cdots \end{pmatrix} \begin{pmatrix} \nu_0 \\ \nu_1 \\ \nu_2 \\ \nu_3 \end{pmatrix}, \quad (55)$$

where again $\tan 2\theta = 2\epsilon_2/\epsilon_1$.

In the VLW case, the parameter ϵ_1 is negligibly small if the solar oscillations are maximal, and can be taken as zero without affecting the phenomenology. If this is done, then reference to the mass matrix shows that both ν_e and ν_τ derive their masses entirely from flavor non-diagonal couplings, and they are maximally mixed (analogous to the ν_μ – ν_s system). Also, if ϵ_1 is taken as zero, then there are only four independent parameters needed in the mass

matrix, and just two in the mixing matrix. The derived θ parameter becomes $\pm\frac{\pi}{4}$, and the mixing matrix becomes very simple:

$$U \simeq \frac{1}{\sqrt{2}} \begin{pmatrix} \cdots & \cdots & -1 & 1 \\ \pm 1 & 1 & \epsilon_3 & \epsilon_3 \\ \mp \epsilon_3 & -\epsilon_3 & 1 & 1 \\ -1 & \pm 1 & \cdots & \cdots \end{pmatrix} \quad (56)$$

5.3 Solar $\nu_e \rightarrow \nu_s$ and $\nu_e \rightarrow \nu_\tau$ oscillations

A more general scenario which is a mixture of the previous two is for solar neutrinos to undergo both $\nu_e \rightarrow \nu_s$ and $\nu_e \rightarrow \nu_\tau$ oscillations. This is easily parameterized by replacing the ν_s and ν_τ states in Eq. (53) with the rotated states ν'_s and ν'_τ and defining

$$\begin{pmatrix} \nu'_s \\ \nu'_\tau \end{pmatrix} = \begin{pmatrix} \cos \alpha & -\sin \alpha \\ \sin \alpha & \cos \alpha \end{pmatrix} \begin{pmatrix} \nu_s \\ \nu_\tau \end{pmatrix}. \quad (57)$$

Then the mass matrix in the $(\nu_s, \nu_e, \nu_\mu, \nu_\tau)$ basis becomes

$$M = m \begin{pmatrix} \epsilon_1 \cos^2 \alpha + \epsilon_4 \sin^2 \alpha & \epsilon_2 \cos \alpha + \epsilon_3 \sin \alpha & \sin \alpha & (\epsilon_4 - \epsilon_1) \sin \alpha \cos \alpha \\ \epsilon_2 \cos \alpha + \epsilon_3 \sin \alpha & 0 & 0 & \epsilon_3 \cos \alpha - \epsilon_2 \sin \alpha \\ \sin \alpha & 0 & \epsilon_4 & \cos \alpha \\ (\epsilon_4 - \epsilon_1) \sin \alpha \cos \alpha & \epsilon_3 \cos \alpha - \epsilon_2 \sin \alpha & \cos \alpha & \epsilon_4 \cos^2 \alpha + \epsilon_1 \sin^2 \alpha \end{pmatrix}, \quad (58)$$

and the matrix which diagonalizes M is

$$\begin{pmatrix} \nu_s \\ \nu_e \\ \nu_\mu \\ \nu_\tau \end{pmatrix} = U \begin{pmatrix} \nu_0 \\ \nu_1 \\ \nu_2 \\ \nu_3 \end{pmatrix} = \begin{pmatrix} \cos \theta \cos \alpha & -\sin \theta \cos \alpha & -\frac{1}{\sqrt{2}} \sin \alpha & \frac{1}{\sqrt{2}} \sin \alpha \\ \sin \theta & \cos \theta & \frac{1}{\sqrt{2}} \epsilon_3 & \frac{1}{\sqrt{2}} \epsilon_3 \\ -\epsilon_3 \sin \theta & -\epsilon_3 \cos \theta & \frac{1}{\sqrt{2}} & \frac{1}{\sqrt{2}} \\ -\cos \theta \sin \alpha & \sin \theta \sin \alpha & -\frac{1}{\sqrt{2}} \cos \alpha & \frac{1}{\sqrt{2}} \cos \alpha \end{pmatrix} \begin{pmatrix} \nu_0 \\ \nu_1 \\ \nu_2 \\ \nu_3 \end{pmatrix}, \quad (59)$$

where $\tan 2\theta = 2\epsilon_2/\epsilon_1$ as before.

6 Oscillation probabilities

6.1 Expressions for any baseline

For the mixing in Eq. (53) (when the solar oscillations are $\nu_e \rightarrow \nu_s$), the off-diagonal vacuum oscillation probabilities obtained from Eq. (2), to leading order in ϵ_j for each Δ_{ij} and ignoring amplitudes smaller than $\mathcal{O}(\epsilon_j^2)$, are

$$P(\nu_e \leftrightarrow \nu_\mu) \simeq \epsilon_3^2 \left[2 \cos^2 \theta (\sin^2 \Delta_{21} + \sin^2 \Delta_{31}) - \sin^2 \Delta_{32} + 2 \sin^2 \theta (\sin^2 \Delta_{20} + \sin^2 \Delta_{30}) - \sin^2 2\theta \sin^2 \Delta_{01} \right], \quad (60)$$

$$P(\nu_e \leftrightarrow \nu_\tau) \simeq \epsilon_3^2 \sin^2 \Delta_{32}, \quad (61)$$

$$P(\nu_e \leftrightarrow \nu_s) \simeq \sin^2 2\theta \sin^2 \Delta_{01}, \quad (62)$$

$$P(\nu_\mu \leftrightarrow \nu_\tau) \simeq \sin^2 \Delta_{32}, \quad (63)$$

$$P(\nu_\mu \leftrightarrow \nu_s) \simeq \sin^2 2\theta \epsilon_3^2 \sin^2 \Delta_{01}, \quad (64)$$

where $\Delta_{01} \ll \Delta_{32} \ll \Delta_{20} \simeq \Delta_{30} \simeq \Delta_{21} \simeq \Delta_{31}$ due to the neutrino mass spectrum. In our model, only the $\nu_\tau\text{-}\nu_s$ oscillation is suppressed beyond $\mathcal{O}(\epsilon_j^2)$.

6.2 Short baseline

For small L/E only the leading oscillations $\Delta_{20} \simeq \Delta_{21} \simeq \Delta_{30} \simeq \Delta_{31}$ contribute, and the only appreciable oscillation probability is

$$P(\nu_e \leftrightarrow \nu_\mu) \simeq 4\epsilon_3^2 \sin^2 \Delta , \quad (65)$$

where $\Delta \equiv m^2 L/4E$. From Eq. (65) we can fix two model parameters

$$\delta m_{sbl}^2 = m^2 , \quad A_{sbl}^{\mu e} = 4\epsilon_3^2 . \quad (66)$$

Since the only short-baseline oscillation is $\nu_e \leftrightarrow \nu_\mu$, these models predict the equality of the ν_e disappearance probability, the ν_μ disappearance probability, and the LSND $\nu_\mu \rightarrow \nu_e$ appearance probability in short-baseline experiments.

6.3 Long baseline

For L/E typical to atmospheric or long baseline neutrino experiments, the oscillations in Δ assume their average values. The Δ_{32} oscillation is now evident, and the non-negligible oscillation probabilities in vacuum are

$$P(\nu_\mu \leftrightarrow \nu_\tau) \simeq \sin^2 \Delta_{32} , \quad (67)$$

$$P(\nu_e \leftrightarrow \nu_\mu) \simeq \epsilon_3^2 (2 - \sin^2 \Delta_{32}) , \quad (68)$$

$$P(\nu_e \leftrightarrow \nu_\tau) \simeq \epsilon_3^2 \sin^2 \Delta_{32} . \quad (69)$$

From Eq. (67)

$$\delta m_{atm}^2 = \delta m_{32}^2 \simeq 4m^2 \epsilon_4 , \quad A_{atm}^{\mu\mu} = 1 , \quad (70)$$

which determines another parameter of the model. The model automatically gives maximal oscillations for atmospheric ν_μ 's, while oscillations in other channels are suppressed. The ν_μ maximal mixing is natural in the sense that it results from the large value of the $M_{\nu_\mu\nu_\tau}$ matrix element relative to the diagonal $M_{\nu_\mu\nu_\mu}$ and $M_{\nu_\tau\nu_\tau}$ elements, without any need for fine tuning of the difference $|M_{\nu_\mu\nu_\mu} - M_{\nu_\tau\nu_\tau}|$.

6.4 Extraterrestrial baseline

Finally, for very large $L/E \gg (\delta m_{atm}^2/\text{eV}^2)^{-1} \text{ km/GeV}$, $\sin^2 \Delta_{32}$ averages to $\frac{1}{2}$ and the appreciable oscillations in vacuum are

$$P(\nu_e \leftrightarrow \nu_s) \simeq \sin^2 2\theta \sin^2 \Delta_{01} , \quad (71)$$

$$P(\nu_\mu \leftrightarrow \nu_s) \simeq \epsilon_3^2 \sin^2 2\theta \sin^2 \Delta_{01} , \quad (72)$$

$$P(\nu_e \leftrightarrow \nu_\mu) \simeq \epsilon_3^2 \left[\frac{3}{2} - \sin^2 2\theta \sin^2 \Delta_{01} \right] , \quad (73)$$

$$P(\nu_e \leftrightarrow \nu_\tau) \simeq \frac{1}{2} \epsilon_3^2 , \quad (74)$$

$$P(\nu_\mu \leftrightarrow \nu_\tau) \simeq \frac{1}{2} . \quad (75)$$

The solar data can then be explained if the parameters in vacuum satisfy

$$\text{SAM : } \quad \delta m_{sun}^2 = \delta m_{01}^2 \simeq m^2 \epsilon_1^2, \quad A_{sun}^{e\ell} = \frac{4\epsilon_2^2}{4\epsilon_2^2 + \epsilon_1^2} \simeq \frac{4\epsilon_2^2}{\epsilon_1^2}, \quad (76)$$

$$\text{LAM : } \quad \delta m_{sun}^2 = \delta m_{01}^2 \simeq m^2 \epsilon_1 \sqrt{\epsilon_1^2 + 4\epsilon_2^2}, \quad A_{sun}^{e\ell} = \frac{4\epsilon_2^2}{4\epsilon_2^2 + \epsilon_1^2}, \quad (77)$$

$$\text{VLW : } \quad \delta m_{sun}^2 = \delta m_{01}^2 \simeq 2m^2 \epsilon_2 \epsilon_3 \epsilon_4, \quad A_{sun}^{e\ell} = \frac{4\epsilon_2^2}{4\epsilon_2^2 + \epsilon_1^2} \simeq 1, \quad (78)$$

in the three cases.

6.5 Determination of the parameters

In any of these scenarios in Sec. 5.1-5.3, the parameters m , ϵ_2 , ϵ_3 , ϵ_4 , and ϵ_1 are obtained from the data in exactly the same way, i.e., via Eqs. (66), (70), and (76)-(78). This is a consequence of the ν_s - ν_τ ambiguity. In all cases, the parameters m , ϵ_3 , and ϵ_4 are related to the observables by

$$m^2 = \delta m_{sbl}^2, \quad \epsilon_3^2 = \frac{A_{sbl}^{\mu e}}{4}, \quad \epsilon_4 = \frac{\delta m_{atm}^2}{4\delta m_{sbl}^2}. \quad (79)$$

In the solar sector we have

$$\text{SAM : } \quad \epsilon_1^2 = \frac{\delta m_{sun}^2}{\delta m_{sbl}^2}, \quad \epsilon_2^2 = \frac{A_{sun}^{e\ell} \delta m_{sun}^2}{4\delta m_{sbl}^2}, \quad (80)$$

$$\text{LAM : } \quad \epsilon_1^2 = \frac{\delta m_{sun}^2 \sqrt{1 - A_{sun}^{e\ell}}}{\delta m_{sbl}^2}, \quad \epsilon_2^2 = \frac{\delta m_{sun}^2 A_{sun}^{e\ell}}{4\delta m_{sbl}^2 \sqrt{1 - A_{sun}^{e\ell}}}, \quad (81)$$

$$\text{VLW : } \quad \epsilon_1 \simeq 0, \quad \epsilon_2 = \frac{8\delta m_{sun}^2}{A_{sbl}^{\mu e} \delta m_{atm}^2}. \quad (82)$$

For the specific values $\delta m_{sbl}^2 = 2 \text{ eV}^2$ and $A_{sbl}^{\mu e} = 2.5 \times 10^{-3}$, $\delta m_{atm}^2 = 5 \times 10^{-3} \text{ eV}^2$ and $A_{atm}^{\mu\mu} = 1$, and $\delta m_{sol}^2 = 4 \times 10^{-6} \text{ eV}^2$ and $A_{sun}^{e\ell} = 1 \times 10^{-2}$, the model parameters are given in Table 3. If we take instead $\delta m_{sbl}^2 = 0.3 \text{ eV}^2$ and $A_{sbl}^{\mu e} = 4.0 \times 10^{-2}$ (which gives the smallest value of δm_{sbl}^2 allowed by the data), we get the model parameters shown in Table 4. In either of these two examples, the δm^2 scale for the atmospheric neutrino oscillation can be adjusted simply by varying ϵ_4 . Also in either case, the two heaviest masses provide relic neutrino targets for a mechanism that may generate the cosmic ray air showers observed above $\gtrsim 10^{20} \text{ eV}$ [50]. We note that the model parameters in Tables 3 and 4 obey the hierarchies described in Eqs. (47)-(49).

7 Model predictions

7.1 Resolving the ν_τ vs. ν_s ambiguity

If the solar oscillations are $\nu_e \rightarrow \nu_s$ as described in Sec. 5.1, then our four-neutrino model predicts that the atmospheric oscillations are $\nu_\mu \rightarrow \nu_\tau$. On the other hand if the solar oscillations are $\nu_e \rightarrow \nu_\tau$ as in Sec. 5.2, the atmospheric oscillations are $\nu_\mu \rightarrow \nu_s$. Several possibilities have been discussed to resolve the ambiguous assignment of ν_τ and ν_s as the oscillation partners of the ν_e 's in the sun and the ν_μ 's in the atmosphere. The Solar Neutrino Observatory (SNO) [51], which can measure both charge-current (CC) and neutral-current

(NC) interactions, will be able to test whether the solar ν_e 's oscillate to sterile or active neutrinos: in the sterile case the CC/NC ratio in SNO will be unity and both CC and NC rates will be suppressed from the SSM predictions, while in the active case only the CC rate is suppressed. Of course if the CC measurement is consistent with the NC, one needs additional evidence to rule out the possibility that the SSM is in error. For instance, SuperKamiokande and SNO can also accurately measure the shape of the ${}^8\text{B}$ neutrino spectrum, which would be distorted by oscillations. Also, a measurement of lower energy neutrinos, such as by the BOREXINO experiment [52], could also be used to detect deviations from the SSM spectrum.

Turning to the atmospheric data, the possibilities to resolve the ambiguity center around the earth-matter effects which are possible in the ν_μ - ν_s oscillation channel but not in the ν_μ - ν_τ channel; there is a relative phase difference between ν_μ and ν_s due to neutral current forward scattering, but there is no phase difference between ν_μ and ν_τ . The analytical analysis of matter-effects involving active and sterile neutrinos can be somewhat complicated [20], but the Schrödinger-like evolution equations can always be solved numerically [53]. Other tests have been proposed recently to resolve the ν_τ - ν_s ambiguity. One test is to measure the asymmetry between downward-going and upward-coming events, for electrons and muons separately [54]. Various oscillation scenarios give rise to dramatically differing trajectories of the asymmetries versus energy for muons and electrons. The preliminary data from SuperK for the individual muon and electron asymmetries suggests again that the atmospheric anomaly is primarily due to ν_μ oscillating into either ν_τ or ν_s , but not ν_e . By eventually measuring an up-down asymmetry for neutral current (NC) events (e.g. $\nu N \rightarrow \nu N \pi^0$), the ambiguity can be resolved: for the ν_τ case there is no NC asymmetry, whereas for the ν_s case there is a large NC asymmetry, as shown in Ref. [55]. The ratio of the rates of NC events relative to the charged current (CC) events can be also used to the same end [56], as can multi-ring events [57]. Searches for muon-less events which come from ν_τ , in association with a ν_μ disappearance measurement, can also in principle distinguish between ν_τ and ν_s [58].

7.2 New oscillation signals

Assuming that the solar oscillations are $\nu_e \rightarrow \nu_s$, we can determine the new oscillation signals predicted by the model. Given the order of magnitude of the δm_{ij}^2 and $U_{\alpha j}$, observable new phenomenology occurs for $L/E \gg 1$ km/GeV in the oscillation channels

$$P(\nu_e \leftrightarrow \nu_\mu) \simeq \frac{1}{4} A_{sbl}^{\mu e} (2 - \sin^2 \Delta_{atm}) , \quad (83)$$

$$P(\nu_e \leftrightarrow \nu_\tau) \simeq \frac{1}{4} A_{sbl}^{\mu e} \sin^2 \Delta_{atm} , \quad (84)$$

where $A_{sbl}^{\mu e} \sim \mathcal{O}(1\%)$ is the oscillation amplitude which describes the LSND results and $\Delta_{atm} = 1.27 \delta m_{atm}^2 L/E \sim (\delta m_{atm}^2 / 5 \times 10^{-3} \text{ eV}^2)(L/157\text{km})(\text{GeV}/E)$ is the oscillation argument which describes the atmospheric neutrino data. We emphasize the new predictions in the $\nu_e \leftrightarrow \nu_\mu$ and $\nu_e \leftrightarrow \nu_\tau$ channels: long baseline oscillations with common oscillation length determined by the *atmospheric* Δ_{atm} and common amplitude given by $\frac{1}{4}$ times the *LSND* amplitude $A_{sbl}^{\mu e}$. These oscillations are in addition to the $\nu_\mu \leftrightarrow \nu_e$ oscillations due to Δ_{sbl} in Eq. (65), which average to the value of $\frac{1}{2} A_{sbl}^{\mu e}$ in a long baseline experiment. The amplitudes

and lengths of these new oscillations complement the set in Table 2, which are inevitable, given the present data, and are therefore required in any model.

How can the oscillation probabilities in Eqs. (83) and (84) be tested? A list of experiments currently underway or being planned to test neutrino oscillation hypotheses is given in Table 5 [59]. In each case the oscillation channel and the parameters which are expected to be tested are shown.

The MINOS experiment [60] can detect $\nu_\mu \rightarrow \nu_e$ or $\nu_\mu \rightarrow \nu_\tau$ oscillations and is sensitive down to $\delta m^2 \simeq 10^{-3} \text{ eV}^2$ and a mixing amplitude of 10^{-2} , which partially overlaps the region of interest; see Fig. 8. If the MINOS experiment can increase its sensitivity, it will provide an even better test of this new phenomenology.

Long-baseline experiments with an intense ν_e or $\bar{\nu}_e$ neutrino beam and which can detect τ 's can see the $\nu_e \rightarrow \nu_\tau$ oscillations in Eq. (84) and provide a definitive test of the new phenomenology predicted by the model. High intensity muon sources [61] can provide simultaneous high intensity ν_μ and $\bar{\nu}_e$ (or $\bar{\nu}_\mu$ and ν_e for antimuons) beams with well-determined fluxes, which could then be aimed at a neutrino detector at a distant site. It is expected that τ 's will be detected through their μ decay mode and that a charge determination can be made, so that one can tell if the τ originated from $\nu_\mu \rightarrow \nu_\tau$ or $\bar{\nu}_e \rightarrow \bar{\nu}_\tau$ oscillations. Current proposals [61] consider SOUDAN ($L = 732 \text{ km}$) or GRAN SASSO ($L = 9900 \text{ km}$) as the far site from an intense muon source at Fermilab (MC). These experiments could also observe $\nu_e \rightarrow \nu_\mu$ oscillations via detection of “wrong-sign” muons, i.e., those with sign opposite to that expected from the ν_μ or $\bar{\nu}_\mu$ source. The neutrino energies are in the 10–50 GeV range. Assuming that low backgrounds can be achieved, the sensitivity to δm^2 is roughly proportional to the inverse square root of the detector size (given the same neutrino energy spectrum at the source); the δm^2 sensitivity does not depend on detector distance L because although the flux in the detector falls off with L^2 , the oscillation argument grows with L^2 for small $\delta m^2 L/E$. For 20 GeV muons at Fermilab and a 10 kT detector at either SOUDAN or GRAN SASSO, the single-event δm^2 sensitivity for $\nu_e \rightarrow \nu_\tau$ oscillations is about $8 \times 10^{-5} \text{ eV}^2$ for maximal mixing [61]. For large δm^2 , the oscillation amplitude single-event sensitivity is roughly inversely proportional to the neutrino flux at the detector divided by the detector size; about 6×10^{-5} for SOUDAN and 10^{-2} for GRAN SASSO [61]. In general, the closer detector has comparable δm^2 sensitivity but better A sensitivity.

The model predicts $\nu_e \rightarrow \nu_\tau$ oscillations with amplitude $\frac{1}{4}A_{sbl}$ (which ranges from 0.0006 to 0.01) and mass-squared difference of δm_{atm}^2 (which ranges from 3×10^{-4} to $7 \times 10^{-3} \text{ eV}^2$). The region of possible $\nu_e \rightarrow \nu_\tau$ oscillations in our model and the regions which can be tested at the SOUDAN and GRAN SASSO sites with a neutrino beam from a high-intensity muon source at Fermilab are shown schematically in Fig. 8, along with the favored parameters for the LSND, atmospheric neutrino, and solar neutrino oscillations. Such experiments would be sensitive to some of the $\nu_e \rightarrow \nu_\tau$ region, though they may not cover the low-mass, small-amplitude part. These searches would also be able to test the $\nu_e \rightarrow \nu_\mu$ oscillations in Eq. (83) and the atmospheric $\nu_\mu \rightarrow \nu_\tau$ oscillations. Additionally, long baseline experiments to the AMANDA detector [62] from Fermilab ($L \simeq 11700 \text{ km}$) or KEK ($L \simeq 11300 \text{ km}$) may be useful in probing oscillations with small δm^2 .

If the solar oscillations are $\nu_e \rightarrow \nu_\tau$, then the oscillations of atmospheric neutrinos are $\nu_\mu \rightarrow \nu_s$ and the new oscillations in Eq. (84) are instead $\nu_e \rightarrow \nu_s$. Neither of these signals would be detectable in long-baseline experiments since the signal is ν_e or ν_μ disappearance

at the few percent level or less. The only measurable signal of the model in this case is the $\nu_e \rightarrow \nu_\mu$ oscillations in Eq. (83).

If the solar neutrinos oscillate into both ν_s and ν_τ as given by the mixing in Eq. (59), any vacuum oscillation in Secs. 6.1-6.4 which has ν_s as the final state is replaced by oscillations to ν_s with relative probability $\cos^2 \alpha$ and to ν_τ with relative probability $\sin^2 \alpha$. Conversely, any oscillation which has ν_τ as the final state is replaced by oscillations to ν_s with relative probability $\sin^2 \alpha$ and to ν_τ with relative probability $\cos^2 \alpha$. In particular, a solar ν_e oscillates into a mixture of ν_s and ν_τ with relative probability $\cos^2 \alpha$ and $\sin^2 \alpha$, respectively, in a vacuum, and an atmospheric ν_μ oscillates into a mixture of ν_s and ν_τ with relative probability $\sin^2 \alpha$ and $\cos^2 \alpha$, respectively, in a vacuum. The new oscillation signal in Eq. (84) for long baseline experiments is replaced by

$$P(\nu_e \leftrightarrow \nu_\tau) \simeq \frac{1}{4} A_{sbl}^{\mu e} \cos^2 \alpha \sin^2 \Delta_{atm} , \quad (85)$$

$$P(\nu_e \leftrightarrow \nu_s) \simeq \frac{1}{4} A_{sbl}^{\mu e} \sin^2 \alpha \sin^2 \Delta_{atm} . \quad (86)$$

Also, there are new oscillations between ν_s and ν_τ , with the general probability for any baseline given by

$$P(\nu_s \rightarrow \nu_\tau) = \sin^2 \alpha \cos^2 \alpha \left[2 \cos^2 \theta (\sin^2 \Delta_{20} + \sin^2 \Delta_{30}) + 2 \sin^2 \theta (\sin^2 \Delta_{21} + \sin^2 \Delta_{31}) - \sin^2 \Delta_{32} - \sin^2 2\theta \sin^2 \Delta_{01} \right] . \quad (87)$$

7.3 Neutrinoless double- β decay

Since the $M_{\nu_e \nu_e}$ mass matrix element is zero in Eq. (45), there is no neutrinoless double- β decay at tree level in our model. The present limit on $M_{\nu_e \nu_e}$ from this process is ~ 0.5 eV [63]. New experiments are under development which may measure $M_{\nu_e \nu_e}$ down as low as 0.01 eV [63]. If a nonzero $M_{\nu_e \nu_e}$ is found at these levels, it would be incompatible with the solar solutions in our models.

7.4 Tritium decay

If ν_e is primarily associated with the lighter pair in the 2+2 model, and $m_1 < m_0 \ll m_2, m_3$, then there will be no measurable effect in the endpoint of the tritium decay spectrum. Since only mass-squared differences are important for oscillations, the inverted 2+2 model, where $m_2, m_3 \ll m_1 < m_0$, is equally viable, although it is not derivable from the mass matrix in Sec. 5. Then the ν_e will have an effective mass of 0.55 – 1.4 eV, which is just below the current limit [64].

7.5 Hot dark matter

For $m \simeq 1.4$ eV, approximately the largest value allowed by the LSND data, $\sum m_\nu \simeq 3$ eV, which according to recent work on early universe formation of the largest structures provides an ideal hot dark matter component [65]. For $m \simeq 0.55$ eV, the contribution to hot dark matter is much smaller. The contribution of the neutrinos to the mass density of the universe is given by $\Omega_\nu = \sum m_\nu / (h^2 93 \text{ eV})$, where h is the Hubble expansion parameter in units of 100

km/s/Mpc [66]; with $h = 0.65$ our model implies $\Omega_\nu \simeq 0.05$. An interesting test of neutrino masses is the power spectrum of early galaxy sizes, to be provided by the Sloan Digital Sky Survey (SDSS) [67]. For two nearly degenerate massive neutrino species, sensitivity down to about 0.2 to 0.9 eV (depending on Ω and h) is expected, providing coverage of all or part of the LSND allowed range ($m = 0.55$ to 1.4 eV in our model). Also, the future MAP [68] and PLANCK [69] satellite missions, which will measure the cosmic microwave background radiation, should be sensitive to neutrino densities to high precision [70], and in particular to the $\nu_\mu \rightarrow \nu_s$ atmospheric or the $\nu_e \rightarrow \nu_s$ large-angle MSW neutrino mixing solutions [71].

7.6 Resonant enhancement in matter

The curves in Fig. 8 (in the scenario where the solar oscillations are $\nu_e \rightarrow \nu_s$) assume vacuum oscillations in the Earth. In general, large corrections to oscillations involving ν_e and ν_s are possible due to matter. The ν_e diagonal element in the effective mass-squared matrix receives an additional term $\sqrt{2}G_F N_e E$ from its forward elastic CC interaction, and the ν_s diagonal element receives the contribution $G_F N_n E/\sqrt{2}$ (relative to the active neutrinos) because it does not have NC interactions. Here, N_e and N_n denote the electron and neutron number density, respectively. In Table 6 we display the resonant energies in the earth for the various vacuum δm^2 values suggested by the available LSND, atmospheric, and solar data. For neutrinos with energies significantly above E_{res} , oscillations are suppressed; for neutrinos with energies significantly below E_{res} , the matter effect is negligible; at the resonant energy, $A_{mat} = 1$ and the oscillation length is increased by $1/\sqrt{A_{vac}}$.

Some of the resonant energy values in Table 6 are of particular interest. Upcoming neutrinos from the atmosphere or astrophysical sources, with mass at the lower end of the LSND range, can have their oscillations resonantly enhanced by the earth's mantle and/or core. Atmospheric neutrinos below a few GeV and the SAM and LAM pp neutrinos from the sun also appear to be near resonance in the earth's matter. Day–night modulation of the solar flux due to earth–matter effects is expected to discriminate between ν_τ and ν_s solar fluxes [72, 73], while a precise measurement of zenith angle dependence may discriminate between ν_τ and ν_s atmospheric fluxes [74]. Oscillation wavelengths commensurate with the size of the earth's mantle and/or core are especially sensitive.

In our model of Sec. 5.1 with $\nu_\mu \rightarrow \nu_\tau$ atmospheric neutrino oscillations, however, these corrections do not significantly affect the large m_2^2 and m_3^2 mass eigenvalues as long as $E \ll 1$ TeV, and hence only modify the δm_{01}^2 oscillation argument. We have verified this by explicit diagonalization of the mass matrix when matter effects are included. Hence we conclude that the matter corrections to the mass matrix in Eq. (45) probably have no observable consequences in all terrestrial experiments. For large L/E , such as when $E \lesssim 10$ MeV for solar neutrinos, the only significant effect of matter is the usual MSW enhancement of $\nu_e \rightarrow \nu_s$ that leads to the solar neutrino suppression of the ν_e flux; in all other oscillation channels the matter-enhanced amplitudes are at the $\epsilon_{\alpha\beta}^2$ level or smaller. In the models discussed in Secs. 5.2 and 5.3, where there is a $\nu_\tau - \nu_s$ component to the atmospheric oscillation, matter effects as discussed here may be important in terrestrial experiments [20].

8 Discussion and summary

8.1 Distinguishing the three solar solutions

The VLW solar solution may be discriminated from the two MSW solutions by a careful measurement of the solar neutrino spectrum by SuperK and BOREXINO [75], or by determining the amount of seasonal variation of the ${}^7\text{Be}$ and pep neutrinos [76], which can be measured by the BOREXINO experiment. The ${}^8\text{B}$ neutrino spectrum as measured in SuperK and SNO will also be useful in discriminating between the SAM and LAM solutions [77]. The HERON and HELLAZ [78] experiments would be able to measure the pp neutrino energy spectrum, which would also be useful in differentiating the three scenarios.

8.2 Possible ν_τ - ν_s mixing

The general case with ν_s - ν_τ mixing is described in Sec. 5.3. The unmixed cases Eqs. (45) and (54) are obtained in the limits $\alpha \rightarrow 0$ and $\alpha \rightarrow \frac{\pi}{2}$, respectively; distinguishing between the unmixed scenarios is discussed in Sec 7.1. How might non-trivial mixing of ν_τ and ν_s be observed, and how might the mixing angle be deduced? A mixed model would generally have a signature intermediate between the two unmixed signatures [20]; e.g., experiments measuring neutral current events for solar and atmospheric neutrinos would find a result between those expected for ν_τ and ν_s .

8.3 Summary

An analysis of all the available data (short baseline LSND, reactor and accelerator, long baseline atmospheric, and extraterrestrial length solar) in terms of neutrino oscillations leads to the conclusion that three independent oscillation lengths are contributing. This then further requires mixing of at least four light-mass neutrinos. For a four light-mass neutrino universe, we draw the following model-independent conclusions:

- (i) the 1+3 (or 3+1) mass spectrum with a separated mass is disfavored when all the data (LSND, reactor, accelerator, solar, and atmospheric) are considered, leaving a spectrum with two nearly-degenerate pairs as preferred;
- (ii) the neutrino mixing matrix elements satisfy $|U_{e2}/U_{e3}| \simeq |U_{\mu2}/U_{\mu3}|$ if $\delta m_{sbl}^2 \simeq 0.3 \text{ eV}^2$, i.e., the parameters lie near the Bugey ν_e disappearance limit;
- (iii) the relation $|U_{\mu2}| \simeq |U_{\mu3}|$ is inferred from the near-maximal mixing of atmospheric ν_μ 's measured by SuperK, which together with (ii) implies $|U_{e2}| \simeq |U_{e3}|$.

Based upon the apparent need for more than three light neutrinos, we have presented four-neutrino models with three active neutrinos and one sterile neutrino. The models naturally have maximal $\nu_\mu \rightarrow \nu_\tau$ (or $\nu_\mu \rightarrow \nu_s$) oscillations of atmospheric neutrinos and can also explain the solar neutrino and LSND results. The solar solutions can be $\nu_e \rightarrow \nu_s$ or $\nu_e \rightarrow \nu_\tau$, and can be small-angle matter-enhanced, large-angle matter-enhanced, or vacuum long-wavelength oscillations; the increased statistics on the electron energy distribution and day/night differences of the SuperK data [79] may further clarify the allowed regions for the solar solutions. The models predict $\nu_e \leftrightarrow \nu_\tau$ (or $\nu_e \rightarrow \nu_s$) and $\nu_e \leftrightarrow \nu_\mu$ oscillations in long-baseline experiments with $L/E \gg 1 \text{ km/GeV}$ with amplitudes that are determined by the

LSND oscillation amplitude and δm^2 scale determined by the oscillation scale of atmospheric neutrinos. For the $\nu_e \rightarrow \nu_\tau$ case, these oscillations might be seen by experiments based on neutrino beams from an intense muon source at Fermilab with a detector at the SOUDAN or GRAN SASSO sites. The $\nu_\mu \rightarrow \nu_e$ oscillations might be seen by the MINOS experiment or at KEK with detectors at Kamiokande and SuperKamiokande. The models also predict the equality of the ν_e disappearance probability, the ν_μ disappearance probability, and the LSND $\nu_\mu \rightarrow \nu_e$ appearance probability in short-baseline experiments.

9 Acknowledgements

We thank D. Caldwell, R. Foot, P. Krastev, J.G. Learned, S. Petcov, G. Raffelt, J. Stone, and R. Volkas for comments and discussions. This work was supported in part by the U.S. Department of Energy, Division of High Energy Physics, under Grants No. DE-FG02-94ER40817, No. DE-FG05-85ER40226, and No. DE-FG02-95ER40896, and in part by the University of Wisconsin Research Committee with funds granted by the Wisconsin Alumni Research Foundation, the Vanderbilt University Research Council, the University of Hawaii, and the Max Planck Institute for Physics, Munich.

References

- [1] J.N. Bahcall and M.H. Pinsonneault, *Rev. Mod. Phys.* **67**, 781 (1995); J.N. Bahcall, S. Basu, and M.H. Pinsonneault, astro-ph/9805135; the new solar flux calculation in the second reference has not yet been implemented in the solar neutrino analyses.
- [2] B.T. Cleveland *et al.*, *Nucl. Phys. B (Proc. Suppl.)* **38**, 47 (1995); Kamiokande collaboration, Y. Fukuda *et al.*, *Phys. Rev. Lett.* **77**, 1683 (1996); GALLEX Collaboration, W. Hampel *et al.*, *Phys. Lett.* **B388**, 384 (1996); SAGE collaboration, J.N. Abdurashitov *et al.*, *Phys. Rev. Lett.* **77**, 4708 (1996).
- [3] Kamiokande collaboration, K.S. Hirata *et al.*, *Phys. Lett.* **B280**, 146 (1992); Y. Fukuda *et al.*, *Phys. Lett.* **B335**, 237 (1994); IMB collaboration, R. Becker-Szendy *et al.*, *Nucl. Phys. Proc. Suppl.* **38B**, 331 (1995); Soudan-2 collaboration, W.W.M. Allison *et al.*, *Phys. Lett.* **B391**, 491 (1997).
- [4] The Super-Kamiokande Collaboration, talk by E. Kearns in Ref. [8] and hep-ex/9803007; Y. Fukuda *et al.*, hep-ex/9803006 and *Phys. Lett.* **B**, to appear.
- [5] The Super-Kamiokande Collaboration, Y. Fukuda *et al.*, hep-ex/9805006.
- [6] J.G. Learned, S. Pakvasa, and T.J. Weiler, *Phys. Lett.* **B207**, 79 (1988); V. Barger and K. Whisnant, *Phys. Lett.* **B209**, 365 (1988); K. Hidaka, M. Honda, and S. Midorikawa, *Phys. Rev. Lett.* **61**, 1537 (1988).
- [7] Liquid Scintillator Neutrino Detector (LSND) collaboration, C. Athanassopoulos *et al.*, *Phys. Rev. Lett.* **75**, 2650 (1995); *ibid.* **77**, 3082 (1996); nucl-ex/9706006.
- [8] For a recent review, see talks at the ITP Conference on Solar Neutrinos: News About SNUS, Santa Barbara, December 1997 at <http://doug-pc.itp.ucsb.edu/online/snu/schedule.html>
- [9] C.Y. Cardall and G.M. Fuller, *Nucl. Phys. Proc. Suppl.* **51B**, 259 (1996); G.L. Fogli, E. Lisi, D. Montanino, and G. Scioscia, *Phys. Rev.* **D56**, 4365 (1997).
- [10] A. Acker, J.G. Learned, S. Pakvasa and T.J. Weiler, *Phys. Lett.* **B298**, 149 (1992); A. Acker and S. Pakvasa, *Phys. Lett.* **B397**, 209 (1997);
- [11] P.I. Krastev and S.T. Petcov, *Phys. Lett.* **B395**, 69 (1997).
- [12] L.M. Johnson and D. McKay, hep-ph/9805311.
- [13] V. Barger, P. Langacker, J. Leveille, and S. Pakvasa, *Phys. Rev. Lett.* **45**, 692 (1980); Z.G. Berezhiani and R.N. Mohapatra, *Phys. Rev.* **D52**, 6607 (1995); E.J. Chun, A.S. Joshipura and A.Y. Smirnov, *Phys. Lett.* **B357**, 608 (1995), and *Phys. Rev.* **D54**, 4654 (1996); K. Benakli and A.Y. Smirnov, *Phys. Rev. Lett.* **79**, 4314 (1997); J.R. Espinosa, hep-ph/9707541; G. Cleaver, M. Cvetič, J.R. Espinosa, L. Everett, and P. Langacker, *Phys. Rev.* **D57**, 2701 (1998); P. Langacker, hep-ph/9805281.

- [14] LEP Electroweak Working Group and SLD Heavy Flavor Group, D. Abbaneo *et al.*, CERN-PPE-96-183, December 1996.
- [15] D.O. Caldwell and R.N. Mohapatra, Phys. Rev. **D 48**, 3259 (1993); J.T. Peltoniemi and J.W.F. Valle, Nucl. Phys. **B 406**, 409 (1993); R. Foot and R.R. Volkas, Phys. Rev. **D 52**, 6595 (1995); Ernest Ma and Probir Roy, Phys. Rev. **D 52**, R4780 (1995); J.J. Gomez-Cadenas and M.C. Gonzalez-Garcia, Z. Phys. **C 71**, 443 (1996); N. Okada and O. Yasuda, Int. J. Mod. Phys. **A 12**, 3669 (1997); S.M. Bilenky, C. Giunti, and W. Grimus, hep-ph/9711416; R.N. Mohapatra, hep-ph/9711444; N. Gaur, A. Ghosal, Ernest Ma, and Probir Roy, hep-ph/9806272; particularly strong enthusiasm for the sterile neutrino is expressed by D.O. Caldwell, hep-ph/9804367.
- [16] R. Barbieri and A. Dolgov, Phys. Lett. **B237**, 440 (1990); K. Enqvist, K. Kainulainen, and M. Thomson, Nucl. Phys. **B373**, 498 (1992); X. Shi, D.N. Schramm, and B.D. Fields, Phys. Rev. **D 48**, 2563 (1993); C.Y. Cardall and G.M. Fuller, Phys. Rev. **D 54**, 1260 (1996); D.P. Kirilova and M.V. Chizhov, hep-ph/9707282; S.M. Bilenky, C. Giunti, W. Grimus and T. Schwetz, hep-ph/9804421.
- [17] P.J. Kernan and S. Sarkar, Phys. Rev. **54**, R3681 (1996); S. Sarkar, *Reports on Progress in Physics* **59**, 1 (1996); K.A. Olive, talk at 5th International Workshop on Topics in Astroparticle and Underground Physics (TAUP 97), Gran Sasso, Italy, 1997; K.A. Olive, proc. of 5th International Conference on Physics Beyond the Standard Model, Balholm, Norway, 1997; C.J. Copi, D.N. Schramm and M.S. Turner, Phys. Rev. Lett. **75**, 3981 (1995); K.A. Olive and G. Steigman, Phys. Lett. **B354**, 357 (1995).
- [18] R. Foot and R.R. Volkas, Phys. Rev. Lett. **75**, 4350 (1995); R. Foot, M.J. Thompson, and R.R. Volkas, Phys. Rev. **D 53**, 5349 (1996); N.F. Bell, R. Foot, and R.R. Volkas, hep-ph/9805259.
- [19] R. Foot and R.R. Volkas, Phys. Rev. **D55**, 5147 (1997);
- [20] Q.Y. Liu and A. Yu. Smirnov, hep-ph/9712493.
- [21] L. Wolfenstein, Phys. Rev. **D 17**, 2369 (1978);
- [22] S.P. Mikheyev and A. Smirnov, Yad. Fiz. **42**, 1441 (1985); Nuovo Cim. **9C**, 17 (1986).
- [23] S.P. Rosen and J.M. Gelb, Phys. Rev. **D 34**, 969 (1986).
- [24] S.J. Parke, Phys. Rev. Lett. **57**, 1275 (1986); S.J. Parke and T.P. Walker, Phys. Rev. Lett. **57**, 2322 (1986); W.C. Haxton, Phys. Rev. Lett. **57**, 1271 (1986); T.K. Kuo and J. Pantaleone, Rev. Mod. Phys. **61**, 937 (1989).
- [25] H. Bethe, Phys. Rev. Lett. **56**, 1305 (1986); V. Barger, R.J.N. Phillips, and K. Whisnant, Phys. Rev. **D 34**, 980 (1986);
- [26] V. Barger, R.J.N. Phillips, and K. Whisnant, Phys. Rev. **D 24**, 538 (1981).
- [27] S.L. Glashow and L.M. Krauss, Phys. Lett. **B190**, 199 (1987).

- [28] V. Barger, K. Whisnant, D. Cline, and R.J.N. Phillips, Phys. Lett. **B93**, 194 (1980).
- [29] L. Borodovsky *et al.*, Phys. Rev. Lett. **68**, 274 (1992).
- [30] KARMEN collaboration, B. Bodmann *et al.*, Nucl. Phys. **A553**, 831c (1993); J. Kleinfeller, Nucl. Phys. **B48** (proc. Suppl.) 207 (1996); talk by B. Armbruster at 33rd Rencontres de Moriond: Electroweak Interactions and Unified Theories, Les Arcs, France, March 1998.
- [31] Y.-Z. Qian *et al.*, Phys. Rev. Lett. **71**, 1965 (1993).
- [32] Y. Declais *et al.*, Nucl. Phys. **B434**, 503 (1995).
- [33] F. Dydak *et al.*, Phys. Lett. **B134**, 281 (1984).
- [34] I.E. Stockdale *et al.*, Phys. Rev. Lett. **52**, 1384 (1984).
- [35] G. Barr, T.K. Gaisser, and T. Stanev, Phys. Rev. **D 39**, 3532 (1989); M. Honda, T. Kajita, K. Kasahara, and S. Midorikawa, Phys. Rev. **D52**, 4985 (1995); V. Agrawal, T.K. Gaisser, P. Lipari, and T. Stanev, Phys. Rev. **D 53**, 1314 (1996); T.K. Gaisser *et al.*, Phys. Rev. **D 54**, 5578 (1996).
- [36] M.C. Gonzalez-Garcia, H. Nunokawa, O. Peres, T. Stanev, and J.W.F. Valle, hep-ph/9801368.
- [37] CHOOZ collaboration, M. Apollonio *et al.*, hep-ex/9711002.
- [38] E. Akhmedov, P. Lipari and M. Lusignoli, Phys. Lett. **B300**, 128 (1993); P. Lipari and M. Lusignoli, hep-ph/9712278, and hep-ph/9803440; R. Foot, R.R. Volkas and O. Yasuda, hep-ph/9801431.
- [39] N. Hata and P. Langacker, Phys. Rev. **D56**, 6107 (1997).
- [40] P. Krastev and S.T. Petcov, Phys. Rev. Lett. **72**, 1960 (1994); Nucl. Phys. **B449**, 605 (1995).
- [41] Y. Totsuka, talk at *Neutrino-98*, Takayama, Japan, June 1998.
- [42] V. Barger, K. Whisnant, S. Pakvasa, and R.J.N. Phillips, Phys. Rev. **D 22**, 2718 (1981).
- [43] P. Langacker, J.P. Leveille, and J. Sheiman, Phys. Rev. **D 27**, 1228 (1983).
- [44] V. Barger, N. Deshpande, P.B. Pal, R.J.N. Phillips, and K. Whisnant, Phys. Rev. **D 43**, 1759 (1991); S. Bludman, D.C. Kennedy, and P. Langacker, Nucl. Phys. **B374**, 373 (1992).
- [45] C. Yanagisawa, talk given at *Pheno 98*, Madison, WI, April 1998.
- [46] V. Barger, K. Whisnant, and T.J. Weiler, hep-ph/9712495 and Phys. Lett. **B**, to appear.
- [47] S.C. Gibbons, R.N. Mohapatra, S. Nandi, and A. Raychaudhuri, hep-ph/9803299.

- [48] S. M. Bilenky, C. Giunti and W. Grimus, Eur. Phys. J. C1, 247 (1998) and hep-ph/9607372.
- [49] This was pointed out to us by G. Raffelt.
- [50] T.J. Weiler, hep-ph/9710431, to appear in Astropart. Phys.
- [51] E. Norman *et al.*, Solar Neutrino Observatory (SNO) collaboration, in proc. of *The Fermilab Conference: DPF 92*, November 1992, Batavia, IL, ed. by C. H. Albright, P.H. Kasper, R. Raja, and J. Yoh (World Scientific, Singapore, 1993), p. 1450.
- [52] BOREXINO Collaboration, C. Arpesella *et al.*, “INFN Borexino proposal,” Vols. I and II, edited by G. Bellini, R. Raghavan *et al.* (Univ. of Milan, 1992); J. Benziger, F.P. Calaprice *et al.*, “Proposal for Participation in the Borexino Solar Neutrino Experiment,” (Princeton University, 1996).
- [53] A.B. Balantekin, J.F. Beacom, and J.M. Fetter, hep-ph/9712390.
- [54] J. Flanagan, J. G. Learned and S. Pakvasa, Phys. Rev. D57, R2649(1998); J. Bunn, R. Foot and R.R. Volkas, Phys. Lett. B413,109(1997).
- [55] J. G. Learned, S. Pakvasa and J. Stone, hep-ph/9805343.
- [56] F. Vissani and A. Smirnov, hep-ph/9710565.
- [57] L.J. Hall and H. Murayama, hep-ph/9806218.
- [58] A. Curioni *et al.*, hep-ph/9805249.
- [59] For World Wide Web links to more information on these and other neutrino oscillation experiments, see the Neutrino Oscillation Industry web page at <http://www.hep.anl.gov/NDK/Hypertext/nuindustry.html>.
- [60] MINOS Collaboration, “Neutrino Oscillation Physics at Fermilab: The NuMI-MINOS Project,” NuMI-L-375, May 1998.
- [61] S. Geer, hep-ph/9712290.
- [62] S. Barwick *et al.*, AMANDA collaboration, in proc. XXVIth International Conference on High Energy Physics, Dallas TX, August 1992, ed. by James R. Sanford (AIP, New York, 1993), p. 1250; F. Halzen, astro-ph/9707289.
- [63] H.V. Klapdor-Kleingrothaus, hep-ph/9802007; J. Phys. **G24**, 483 (1998).
- [64] A.I. Belesev *et al.*, Phys. Lett. **B350**, 263 (1995); V.M. Lobashev *et al.*, in *Proc. of Neutrino '98*, ed. by K. Enqvist, K. Huitu, and J. Maalampi (World Scientific, Singapore, 1997).
- [65] For a recent discussion see J. Primack, astro-ph/9707285.
- [66] E.W. Kolb and M.S. Turner, *The Early Universe* (Addison-Wesley, Reading, 1990).

- [67] W. Hu, D.J. Eisenstein, and M. Tegmark, astro-ph/9712057.
- [68] See <http://map.gsfc.nasa.gov> for information on MAP.
- [69] See <http://astro.estec.esa.nl/Planck/> for information on PLANCK.
- [70] C.-P. Ma and E. Bertschinger, *Astrophys. J.* **455**, 7 (1995); S. Dodelson, E. Gates, and A. Stebbins, *Astrophys. J.* **467**, 10 (1996); R.E. Lopez, S. Dodelson, A. Heckler, and M.S. Turner, astro-ph/9803095.
- [71] S. Hannestad and G. Raffelt, astro-ph/9805223.
- [72] M. Maris and S.T. Petcov, hep-ph/9803244; S.T Petcov, hep-ph/9805262.
- [73] E.K. Akhmedov, hep-ph/9805272.
- [74] Q.Y. Liu, S.P. Mikheyev, and A.Y. Smirnov, hep-ph/9803415.
- [75] B. Faid, G.L. Fogli, E. Lisi, and D. Montanino, hep-ph/9805293.
- [76] V. Barger, R.J.N. Phillips, and K. Whisnant, *Phys. Rev. Lett.* **65**, 3084 (1990).
- [77] G.L. Fogli, E. Lisi, and D. Montanino, hep-ph/9803309.
- [78] HELLAZ Collaboration, F. Arzarello et al., CERN-LAA/94-19.
- [79] Y. Suzuki, talk at *Neutrino-98*, Takayama, Japan, June 1998.

Table 1: Ranges of mass-squared differences and amplitudes that provide oscillation solutions to the solar neutrino data within 95% C.L. in the small-angle MSW, large-angle MSW and vacuum long-wavelength scenarios when $\nu_e \rightarrow \nu_s$ or $\nu_e \rightarrow \nu_\tau$ [39]. The new SuperK data and new solar flux calculations give slightly different oscillation parameters than those quoted here; in particular, the δm^2 values for the VLW solution are higher, of order 4×10^{-10} eV² [41].

$\nu_e \rightarrow \nu_s$	SAM	LAM	VLW
δm^2 (eV ²)	3.5×10^{-6} – 7.5×10^{-6}	$\simeq 9 \times 10^{-6}$	$\simeq 5 \times 10^{-11}$
A_{sun}^{es}	2.5×10^{-3} – 1.6×10^{-2}	$\simeq 0.7$	$\simeq 1$
$\nu_e \rightarrow \nu_\tau$	SAM	LAM	VLW
δm^2 (eV ²)	4×10^{-6} – 9×10^{-6}	8×10^{-6} – 3×10^{-5}	5×10^{-11} – 8×10^{-11}
$A_{sun}^{e\tau}$	3.5×10^{-3} – 1.3×10^{-2}	0.4–0.8	0.6–1.0

Table 2: Some typical δm^2 and vacuum oscillation amplitudes suggested by experiment, and the corresponding vacuum oscillation lengths $\lambda_\nu = 2.5 (E_\nu/\text{GeV})(\delta m^2/\text{eV}^2)^{-1}$ km for representative neutrino energies. Here AU is the earth-sun distance and R_\oplus is the earth's radius.

$\delta m^2/\text{eV}^2$	A	$\lambda_\nu = 4\pi E_\nu/\delta m^2$, with E_ν as shown:							
		5 MeV	100 MeV	2 GeV	10 GeV	30 GeV	100 GeV	1 TeV	
LSND 2	0.0025	6 m	125 m	2.5 km	12 km	37 km	125 km	1250 km	
LSND 0.3	0.04	42 m	840 m	17 km	83 km	250 km	830 km	1.2 R_\oplus	
ATM 5×10^{-3}	0.8–1.0	2.5 km	50 km	10^3 km	5000 km	2.3 R_\oplus	7.8 R_\oplus	78 R_\oplus	
SAM 6×10^{-6}	.0025–.016	2100 km	6.5 R_\oplus	130 R_\oplus					
LAM 10^{-5}	0.4–0.8	1260 km	3.9 R_\oplus	78 R_\oplus					
VLW 5×10^{-11}	0.6–1.0	1.7 AU	33 AU	670 AU					

Table 3: Typical model parameters for the input data $\delta m_{sbl}^2 = 2$ eV², $A_{sbl}^{\mu e} = 2.5 \times 10^{-3}$, $\delta m_{atm}^2 = 5 \times 10^{-3}$ eV², and $A_{atm}^{\mu\mu} = 1$.

inputs	SAM	LAM	VLW
δm_{sun}^2 (eV ²)	4×10^{-6}	9×10^{-6}	5×10^{-11}
$A_{sun}^{e\mu}$	1×10^{-2}	0.72	1.0
outputs	SAM	LAM	VLW
m (eV)	1.4	1.4	1.4
ϵ_3	2.5×10^{-2}	2.5×10^{-2}	2.5×10^{-2}
ϵ_4	6.3×10^{-4}	6.3×10^{-4}	6.3×10^{-4}
ϵ_2	7.1×10^{-5}	1.2×10^{-3}	3.2×10^{-5}
ϵ_1	1.4×10^{-3}	1.5×10^{-3}	$\simeq 0$

Table 4: Typical model parameters for the input data $\delta m_{sbl}^2 = 0.3 \text{ eV}^2$, $A_{sbl}^{\mu e} = 4.0 \times 10^{-2}$, $\delta m_{atm}^2 = 5 \times 10^{-3} \text{ eV}^2$, and $A_{atm}^{\mu\mu} = 1$.

inputs	SAM	LAM	VLW
$\delta m_{sun}^2 \text{ (eV}^2\text{)}$	4×10^{-6}	9×10^{-6}	5×10^{-11}
$A_{sun}^{e\bar{e}}$	1×10^{-2}	0.72	1.0
outputs	SAM	LAM	VLW
$m \text{ (eV)}$	0.55	0.55	0.55
ϵ_3	1.0×10^{-1}	1.0×10^{-1}	1.0×10^{-1}
ϵ_4	4.2×10^{-3}	4.2×10^{-3}	4.2×10^{-3}
ϵ_2	1.9×10^{-4}	3.2×10^{-3}	2.0×10^{-6}
ϵ_1	3.7×10^{-3}	4.0×10^{-3}	$\simeq 0$

Table 5: Current and planned short and long baseline neutrino oscillation experiments. Stars denote accessible oscillation channels. The δm^2 and $\sin^2 2\theta$ sensitivities are given.

Experiment	ν_μ	ν_μ	ν_e	ν_e	δm^2 (eV ²)	$\sin^2 2\theta$	Test LSND?	Test Atmos?	Test Model?	
	\downarrow ν_e	\downarrow ν_τ	\downarrow ν_τ	\downarrow ν_e					ν_μ	ν_e
BOONE	*				10^{-2}	6×10^{-4}	*			
BOREXINO				*	10^{-6}	0.4				
CHORUS		*			0.3	2×10^{-4}				
COSMOS		*			0.1	10^{-5}				
ICARUS, NOE, AQUA-RICH, OPERA	*	*			3×10^{-3}	4×10^{-2}		p		
KARMEN	*				4×10^{-2}	10^{-3}	*			
KamLAND	*				2×10^{-3}	0.2				
K2K	*				2×10^{-3}	5×10^{-2}		p		
MC/Gran Sasso	*	*	*		8×10^{-5}	10^{-2}	p	*	p	p
MC/Soudan	*	*	*		8×10^{-5}	6×10^{-5}	*	*	*	p
MINOS	*	*			10^{-3}	10^{-2}	p	p	p	
NOMAD		*			0.5	3×10^{-4}				
ORLANDO, ESS	*				3×10^{-3}	10^{-4}	*			
Palo Verde				*	10^{-3}	0.2				
TOSCA		*			0.1	10^{-5}				

p = partially

Table 6: Resonant energies $E_{res} = 6.6 \sqrt{1 - A} (\delta m^2 / \text{eV}^2) (N_e / N_A \text{ cm}^{-3})^{-1}$ TeV in the earth's core and mantle for $\nu_e - \nu_{\mu/\tau}$ oscillations, for some typical vacuum values for the δm^2 's and amplitudes suggested by the data. Here A is the oscillation amplitude and N_A is Avagadro's number. We have taken the core electron density to be 4.5 to 6.0 N_A / cm^3 , and the mantle density to be 1.6 to 2.6 N_A / cm^3 . Resonant energies for $\nu_e - \nu_s$ oscillations are $2N_e / (2N_e - N_n)$ times larger than for $\nu_e - \nu_{\mu/\tau}$ oscillations, resonant energies for $\nu_{\mu/\tau} - \nu_s$ oscillations are $2N_e / N_n$ times larger, but resonance occurs for $\bar{\nu}$ rather than ν since the phase difference due to matter has the opposite sign.

A		$\delta m^2 / \text{eV}^2$	$E_{res} = \delta m^2 \sqrt{1 - A} / (2\sqrt{2}G_F N_e)$	
			core	mantle
$\ll 1$	LSND	2	2.2–2.9 TeV	5.1–8.2 TeV
$\ll 1$	LSND	0.3	330–440 GeV	0.8–1.2 TeV
0.8	ATM	5×10^{-3}	2.4–3.3 GeV	5.6–9.2 GeV
$\ll 1$	SAM	6×10^{-6}	6.5–8.8 MeV	15–25 MeV
0.6	LAM	10^{-5}	6.9–9.2 MeV	16–26 MeV
0.8	VLW	5×10^{-10}	25–33 eV	55–90 eV

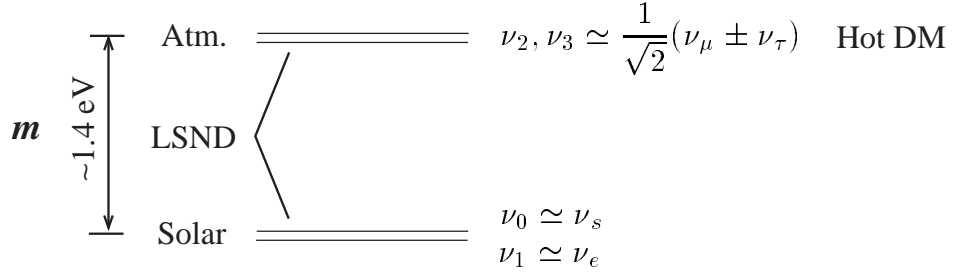


Figure 1: Neutrino mass spectrum, showing a possible flavor assignment for each mass eigenstate, and showing which mass splittings are responsible for the LSND, atmospheric, and solar oscillations.

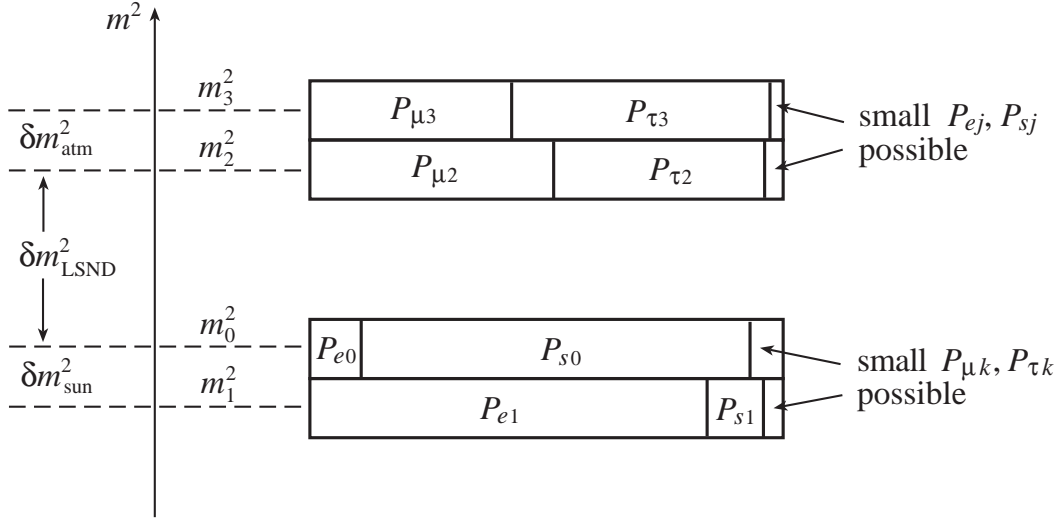


Figure 2: Typical probability rectangles for a 2+2 model where ν_2 and ν_3 generate the atmospheric oscillations and ν_1 and ν_0 generate the solar oscillations. For the non-dominant probabilities $j = 2$ or 3 and $k = 1$ or 0 .

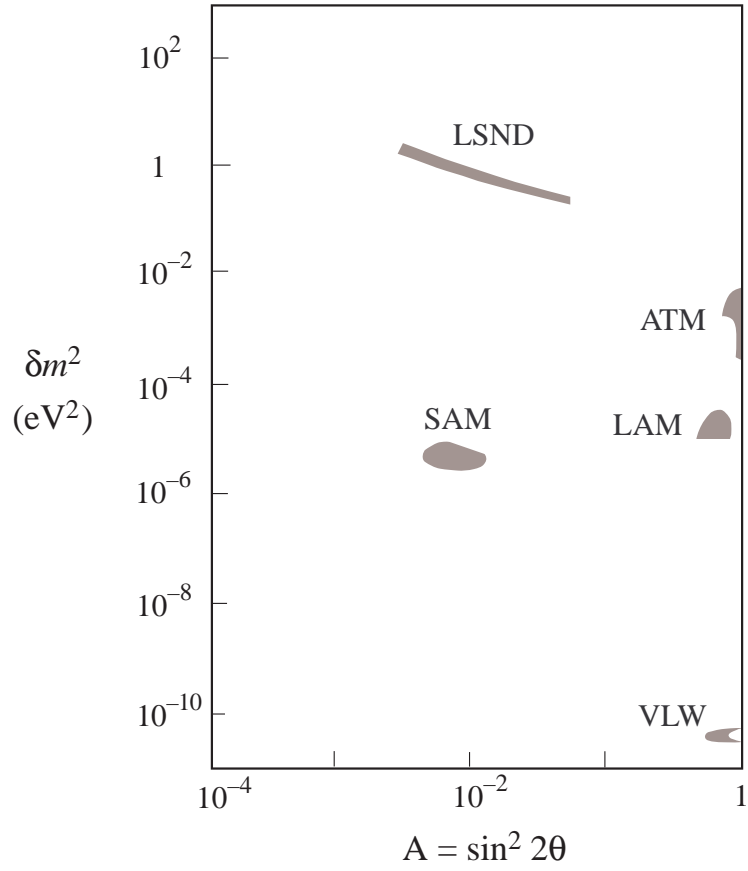
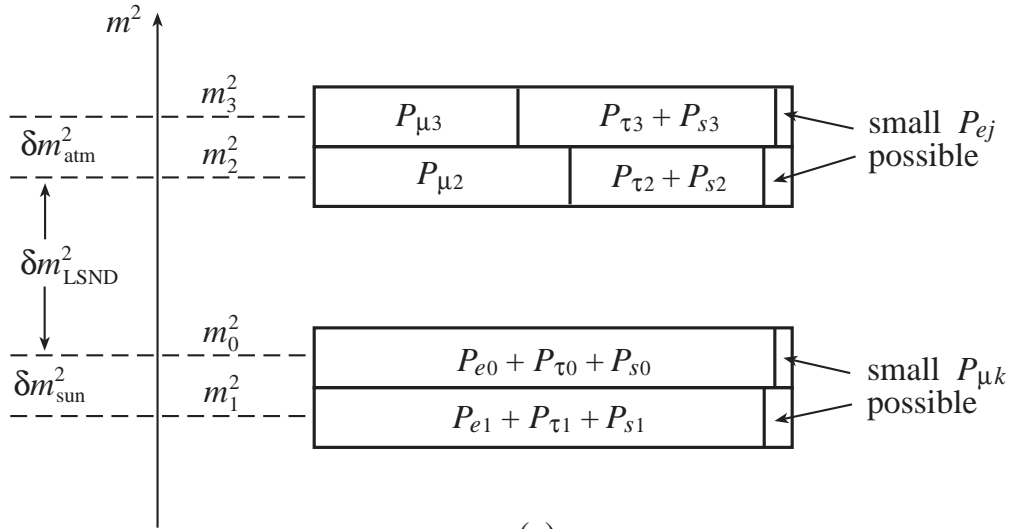
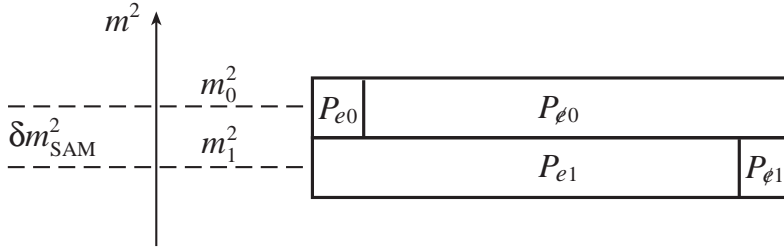


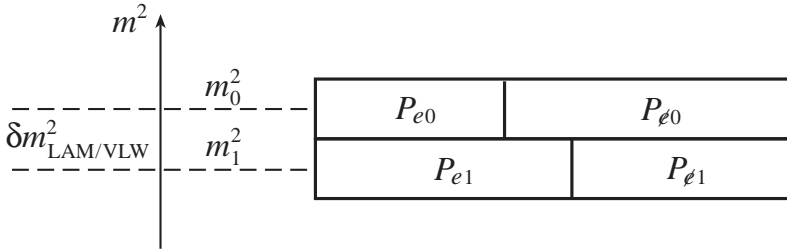
Figure 3: The three allowed two-neutrino solar solutions for $\nu_e \rightarrow \nu_\tau$ oscillations [45]. The corresponding region for $\nu_e \rightarrow \nu_s$ oscillations are similar to the $\nu_e \rightarrow \nu_\tau$ case.



(a)



(b)



(c)

Figure 4: Typical probability rectangles for some 2+2 models. (a) Rectangles deduced from atmospheric and CHOOZ neutrino data, with ν_μ lying predominantly in the ν_2 and ν_3 states with large mixing with either ν_τ and/or ν_s . The $P_{\mu 0}$ and $P_{\mu 1}$ probabilities are small, but the $P_{\mu 0}$ and $P_{\mu 1}$ probabilities are not yet determined. The partitioning of the $P_{\mu 0}$ and $P_{\mu 1}$ probabilities once the solar solution is specified are also shown for the (b) small angle MSW and (c) large angle MSW or vacuum long-wavelength solutions.

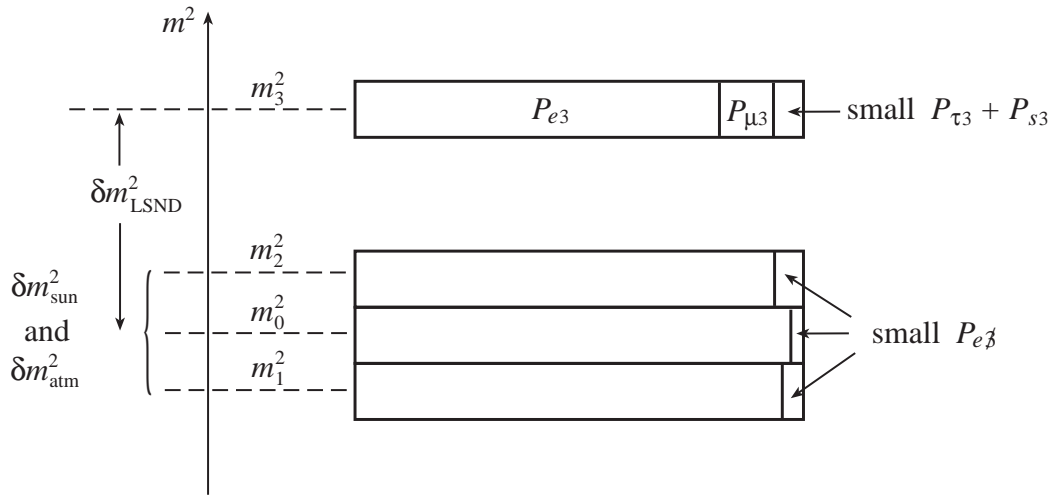


Figure 5: Typical probability rectangles for the 1+3 model when P_{e3} is large and $P_{e\beta}$ is small.

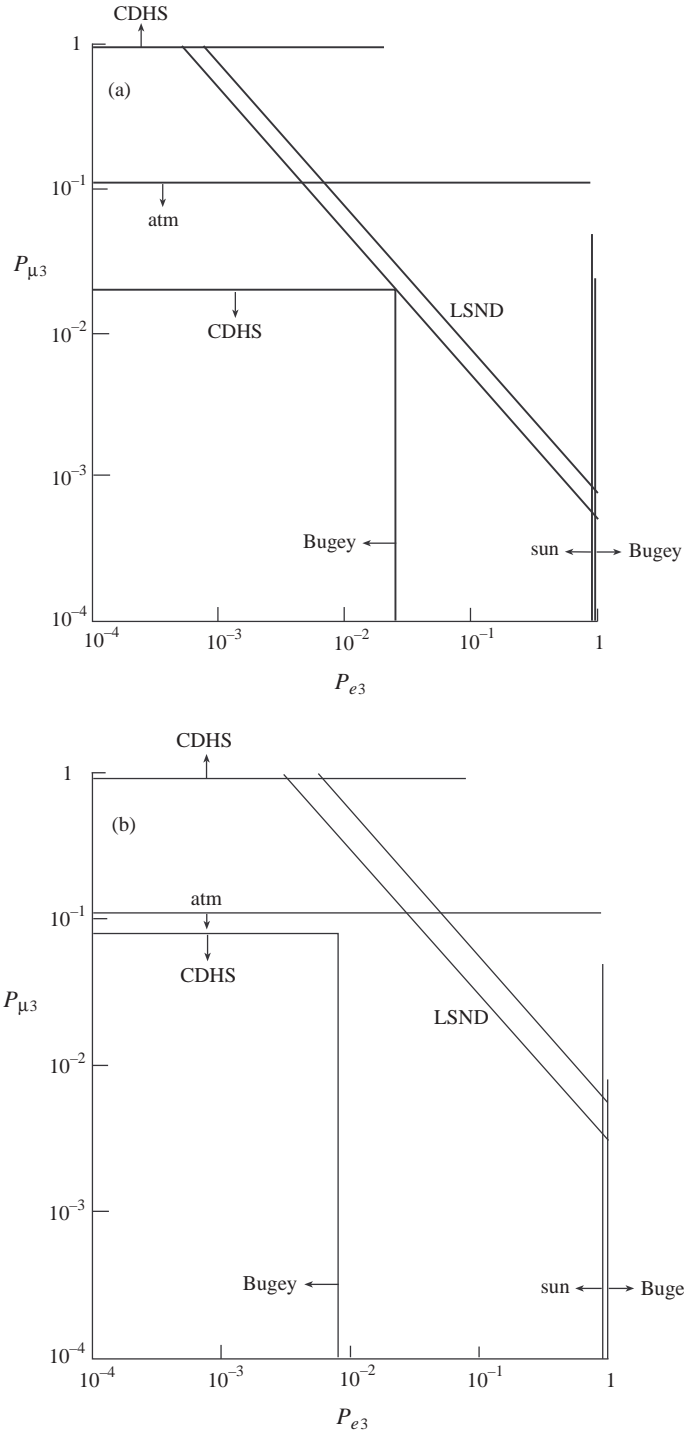


Figure 6: Constraints on $P_{\mu 3}$ and $P_{e 3}$ for the 1+3 model when (a) $\delta m_{sbl}^2 = 1.7 \text{ eV}^2$ and (b) $\delta m_{sbl}^2 = 0.5 \text{ eV}^2$. The LSND, Bugey, CDHS, atmospheric, and solar constraints are obtained by comparison of the appropriate data with Eqs. (19), (20), (21), (22), and (25), respectively. Not displayed is the unitarity constraint $P_{e 3} + P_{\mu 3} \leq 1$.

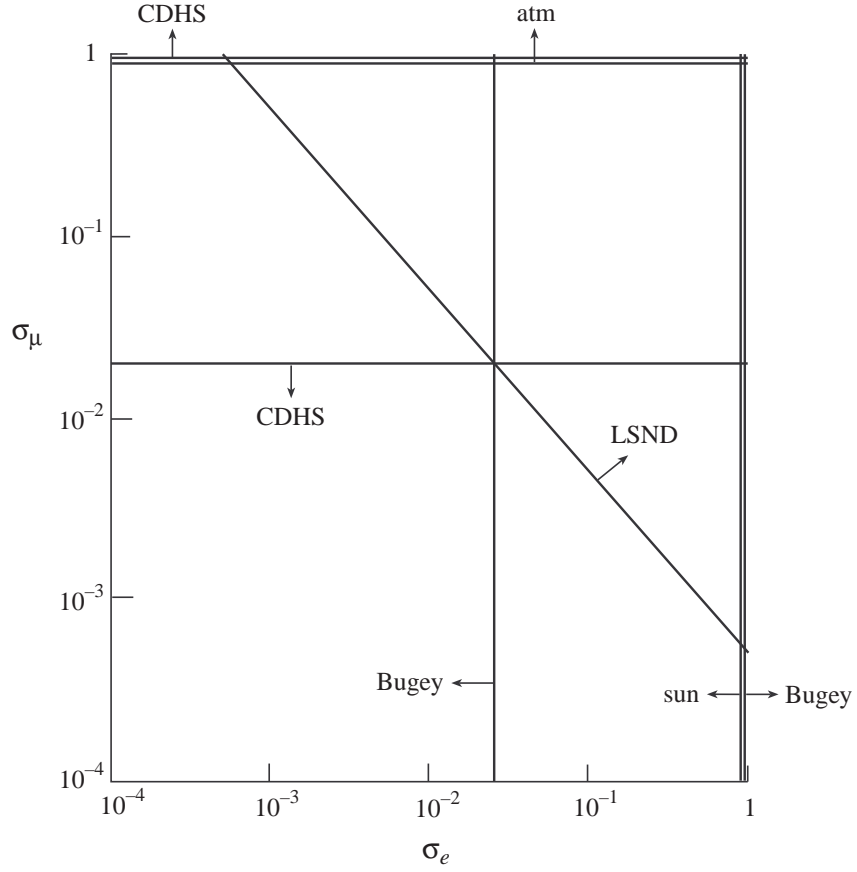


Figure 7: Constraints on σ_μ and σ_e defined in Eq. (31) for the 2+2 model when $\delta m_{sbl}^2 = 1.7 \text{ eV}^2$. The LSND, Bugey, CDHS, solar and atmospheric constraints are obtained by comparison of the appropriate data with Eqs. (32), (29), (30), (33), and (34), respectively.

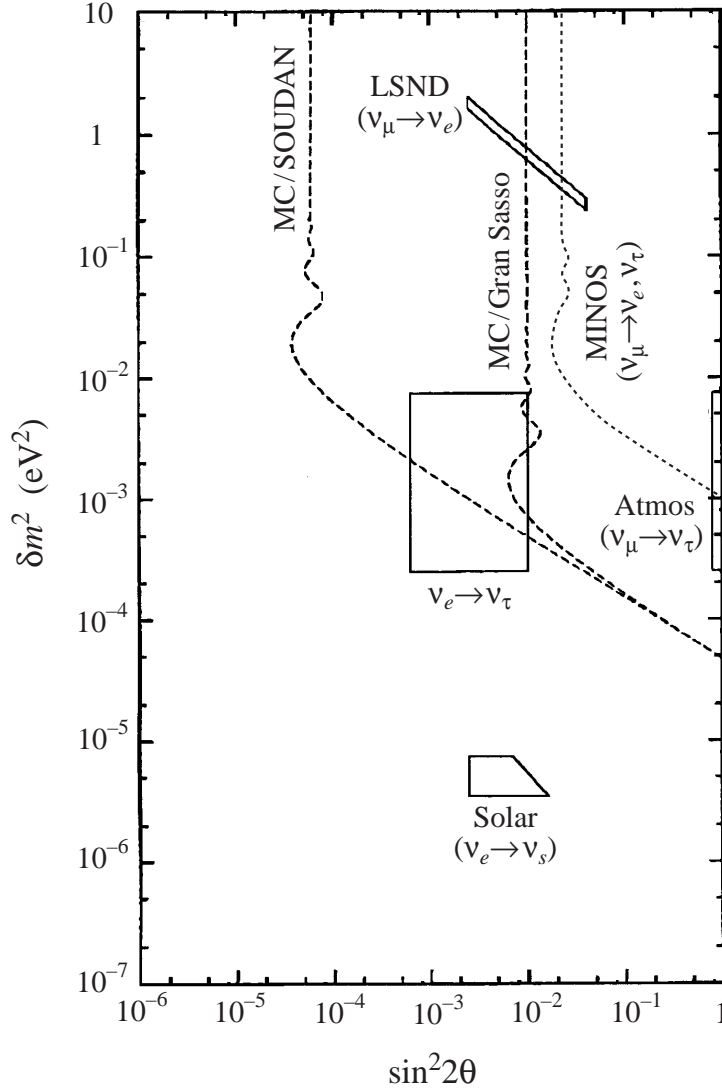


Figure 8: Predicted region in the effective δm^2 - $\sin^2 2\theta$ parameter space for $\nu_e \rightarrow \nu_\tau$ oscillations in the four-neutrino model (solid rectangle), which is determined by $\frac{1}{4}$ of the LSND $\nu_\mu \rightarrow \nu_e$ oscillation amplitude and the atmospheric neutrino $\nu_\mu \rightarrow \nu_\tau$ oscillation δm^2 scale. The dotted curves show the potential limits on $\nu_\mu \rightarrow \nu_e, \nu_\tau$ oscillations from the MINOS experiment [60] and the dashed curves show the potential limits on $\nu_e, \nu_\mu \rightarrow \nu_\tau$ oscillations that can be set by neutrino beams from an intense muon source at Fermilab [61] to detectors at the SOUDAN and GRAN SASSO sites for muons with energy of 20 GeV. Also shown are the parameters for the solar $\nu_e \rightarrow \nu_s$ small-angle MSW oscillation.